A maltol-containing Ruthenium Polypyridyl Complex as a Potential Anticancer Agent

Anna Notaro,[a] Marta Jakubaszek, [a, b] Severin Koch,[c] Riccardo Rubbiani,[c] Orsolya Dömötör, [d] Éva A. Enyedy, [d, e] Mazzarine Dotou, [a] Fethi Bedioui, [f] Mickaël Tharaud, [g] Bruno Goud, [b] Stefano Ferrari, [h,i] Enzo Alessio, [j] and Gilles Gasser*[a]

[a] Chimie ParisTech, PSL University, CNRS, Institute of Chemistry for Life and Health Sciences, Laboratory for Inorganic Chemical Biology, F-75005 Paris, France.

[b] Institut Curie, PSL University, CNRS UMR 144, Paris, France.

[c] Department of Chemistry, University of Zurich, Winterthurerstrasse 190, 8057 Zurich, Switzerland.

[d] Department of Inorganic and Analytical Chemistry, Interdisciplinary Excellence Centre, University of Szeged, Dóm tér 7. H-6720 Szeged, Hungary.

[e] MTA-SZTE Momentum Functional Metal Complexes Research Group, University of Szeged, Dóm tér 7, H-6720 Szeged, Hungary.

[f] Chimie ParisTech, PSL University, CNRS, Institute of Chemistry for Life and Health Sciences, Team Synthèse, Electrochimie, Imagerie et Systèmes Analytiques pour le Diagnostic, F-75005 Paris, France.

[g] Université de Paris, Institut de physique du globe de Paris, CNRS, F-75005 Paris, France.

[h] Institute of Molecular Cancer Research, University of Zurich, Zurich, Switzerland.

[i] Institute of Molecular Genetics of the Czech Academy of Sciences, Videnska 1083, 143 00 Prague, Czech Republic.

[j] Department of Chemical and Pharmaceutical Sciences, University of Trieste, Via L. Giorgieri 1, 34127 Trieste, Italy.

* Corresponding author: E-mail: gilles.gasser@chimeparistech.psl.eu; WWW: www.gassergroup.com; Phone: +33 1 44 27 56 02

ORCID Number

Anna Notaro: 0000-0003-0148-1160

Marta Jakubaszek: 0000-0001-7590-2330

Orsolya Dömötör: 0000-0001-8736-3215

Éva A. Enyedy: 0000-0002-8058-8128

Mazzarine Dotou: 0000-0001-8781-6763

Fethi Bedioui: 0000-0002-0063-4412

Bruno Goud: 0000-0003-1227-4159

Stefano Ferrari: 0000-0002-6607-215X

Enzo Alessio: 0000-0002-4908-9400

Gilles Gasser: 0000-0002-4244-5097

Keywords: Bioinorganic Chemistry, Cancer, DNA, Medicinal Inorganic Chemistry, Ruthenium.

Abstract

Cancer is one of the main causes of death worldwide. Chemotherapy, despite its severe side effects, is to date one of the leading strategies against cancer. Metal-based drugs present several potential advantages when compared to organic ones and gained trust from the scientific community after the approval on the market of the drug cisplatin. Recently, we reported a ruthenium complex (**[Ru(DIP)$_2$(sq)](PF$_6$)**, where DIP is 4,7-diphenyl-1,10-phenantroline and sq is the semiquinonate), with a remarkable potential as chemotherapeutic agent against cancer, both *in vitro* and *in vivo*. In this work, we analyse a structurally similar compound, namely **[Ru(DIP)$_2$(mal)](PF$_6$)**, carrying the flavour-enhancing agent approved by the FDA, maltol (mal). To possess an FDA approved ligand is crucial for a complex, whose mechanism of action might include ligand exchange. Herein, we describe the synthesis and characterisation of **[Ru(DIP)$_2$(mal)](PF$_6$)**, its stability in solutions and in conditions which resemble the physiological ones, and its in-depth biological investigation. Cytotoxicity tests on different cell lines in 2D model and on HeLa MultiCellular Tumour Spheroids (MCTS) demonstrated that our compound has higher activity compared to the approved drug cisplatin, inspiring further tests. **[Ru(DIP)$_2$(mal)](PF$_6$)** was efficiently internalised by HeLa cells through a passive transport mechanism and severely affected the mitochondrial metabolism.

Introduction

Metal-based drugs are currently playing an essential role in the treatment of cancer.[1] Cisplatin, carboplatin and oxaliplatin are widely used in the clinics.[2],[3] Ruthenium complexes are, to date, the most promising candidates for the next generation of metal-based drugs against cancer.[4]–[6] The Ru(III) complexes KP1019, KP1339 (referred as IT-139 recently) and NAMI-A have entered clinical trials as anticancer drugs,[7]–[11] while TLD-1433 – a substitutionally inert Ru(II) polypyridyl complex – recently entered phase II clinical trial as a photosensitizer for photodynamic therapy (PDT).[12],[13] Inert Ru polypyridyl complexes hold a tremendous potential as chemotherapeutic agents against cancer.[14]–[16] Recently, we reported the in-depth biological investigation of a very promising Ru(II) polypyridyl complex carrying a semiquinonate ligand (**$[Ru(DIP)_2(sq)](PF_6)$**) (Figure 1, DIP = 4,7-diphenyl-1,10-phenantroline, sq = semiquinonate).[17] We could notably show that this complex had a much higher cytotoxicity than cisplatin in several cancer cell lines (i.e. in the nanomolar concentration range), and a very promising *in vivo* activity. Moreover, contrary to cisplatin, **$[Ru(DIP)_2(sq)](PF_6)$** results in mitochondrial dysfunction as one of its modes of action.[17]

Maltol, (3-hydroxy-2-methyl-4-pyrone), belonging to the family of 2-alkyl-3-hydroxy-4-pyrones, is structurally very similar to sq and – upon deprotonation – forms stable 5-membered chelate rings with metal ions. Maltol is a product of carbohydrate degradation, which can be found in coffee, baked cereals, chicory, soybeans and other products.[18],[19] It possesses candy-floss, sweet flavour, and is approved by the FDA as a flavour-enhancing agent.[18],[20],[21] Maltol is known for its antioxidative properties[22] and its ability to chelate metal ions. It is an effective ligand for increasing absorption and bioavailability of metal ions.[23],[24],[33],[25]–[32] Maltol has been tested on different

human cell lines, confirming lack of toxicity with IC_{50} (the half maximal inhibitory concentration) values always above 100 μM.[34],[35] In 2006, Thompson and co-workers reported a critical review about the applications of maltol-containing metal complexes in medicinal chemistry.[27] One of them concerns the restoration of iron balance in anaemia. The uptake of iron has indeed been proven to be significantly enhanced in the presence of maltol, in both *in vitro* and *in vivo* models.[36],[37] The bis(maltolato)oxovanadium(IV) complex developed by Orvig and co-workers (better known as **BMOV**, Figure 1) was found to have a high anti-diabetic activity as insulin mimetic agent, and its derivative – the orally administered bis(ethylmaltolato)oxovanadium(IV) (**BEOV** in Figure 1) – was tested in phase IIa.[24],[28],[38]–[41] Gallium maltolate, (tris(3-hydroxy-2-methyl-4H-pyran-4-onato)gallium (**GaM**), Figure 1), recently has completed phase II clinical trials for the treatment of malignant lymphomas, multiple myeloma, bladder neoplasm and prostatic neoplasms.[42]–[45] It was found to be better orally absorbed than simple gallium salts (such as the chloride or nitrate).[42] This higher oral bioavailability offers the possibility of a more convenient and tolerable achievement of therapeutically useful blood gallium levels.[42],[43] The great potential demonstrated by **GaM** led to the investigation of other possible applications of this compound in medicine (e.g., treatment of *Pseudomonas aeruginosa* infection, the neglected tropical disease yaws, and other types of cancer).[46]–[49] Mononuclear and dinuclear maltol-containing half-sandwich ruthenium(II) complexes have been extensively investigated in the past decades as chemotherapeutic agents against cancer.[30],[32],[50],[51] However, only dinuclear species were found to have significant cytotoxicity toward human cancer cell lines (IC_{50} <10 μM).[32],[51]

With this mind, in this work we present a novel Ru(II)-maltol polypyridyl complex, namely **[Ru(DIP)$_2$(mal)](PF$_6$)** (mal = maltolate) shown in Figure 1. To the best of our knowledge, **[Ru(DIP)$_2$(mal)](PF$_6$)** is the first maltol-containing ruthenium polypyridyl complex investigated as a chemotherapeutic agent against cancer. **[Ru(DIP)$_2$(mal)](PF$_6$)** is chiral and is isolated as a racemic mixture of Δ and Λ enantiomers. No attempt to work with enantiopure complexes was made in this work. In this study, besides the synthesis and characterisation of **[Ru(DIP)$_2$(mal)](PF$_6$)**, we report its binding to human serum albumin (HSA) and its biological activity against different human cancer cell lines. Due to the high cytotoxicity expressed by **[Ru(DIP)$_2$(mal)](PF$_6$)**, additional biological studies were undertaken to obtain more insights about the possible targets and mechanism(s) of action of the compound. As described below, **[Ru(DIP)$_2$(mal)](PF$_6$)** was found to be highly cytotoxic against HeLa MCTS (Multicellular tumour spheroids) and to be efficiently internalised by HeLa cells. Its accumulation in cytoplasm, lysosomes, nucleus and mitochondria suggests a mechanism of action involving multicellular targets, which does not exclude ligand exchange at the metal centre.

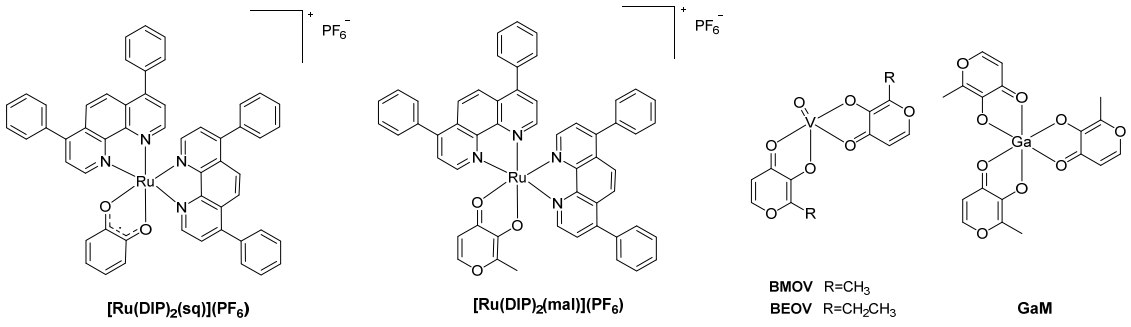

Figure 1. Structures of **[Ru(DIP)$_2$(sq)](PF$_6$)**, **[Ru(DIP)$_2$(mal)](PF$_6$)**, **BMOV**, **BEOV** and **GaM**.

Results and Discussion

Synthesis and characterization of $[Ru(DIP)_2(mal)](PF_6)$

The synthesis of **$[Ru(DIP)_2(mal)](PF_6)$** was achieved in two steps (Scheme 1). In the first step the known Ru(II) precursor $RuCl_2(dmso)_4$[52] was treated with DIP and LiCl in refluxing DMF to afford $RuCl_2(DIP)_2$ in 72% yield after precipitation with acetone.[53] The ruthenium intermediate was then refluxed in ethanol with maltol in the presence of NaOH for 3 h. **$[Ru(DIP)_2(mal)](PF_6)$** was obtained after precipitation with a large excess of NH_4PF_6 in 90% yield. The identity of the product was confirmed by ^1H and ^{13}C NMR spectroscopy (Figure S1) as well as HR-MS, and its purity by microanalysis. The number of resonances showed in the ^1H is consistent with the inequivalence of the two DIP ligands, due to the asymmetry of maltolate.

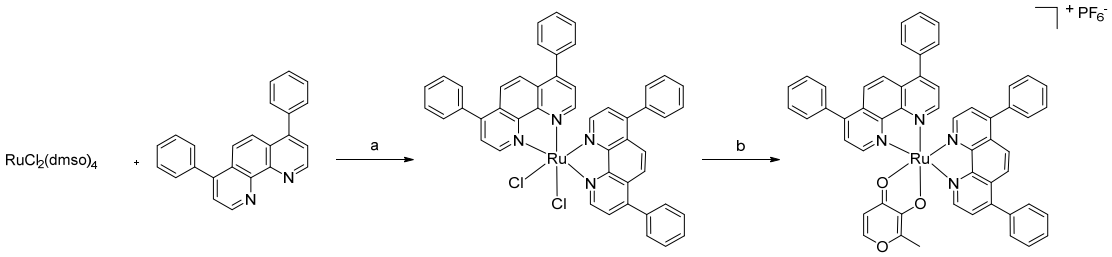

Scheme 1. Synthesis of **$[Ru(DIP)_2(mal)](PF_6)$**. a) LiCl, DMF, reflux, 24 h, 78%; b) (i) NaOH, maltol, ethanol, reflux, 3 h; (ii) NH_4PF_6, ethanol/H_2O (1:10), yield: 90%.

Electrochemistry

The electrochemical properties of **$[Ru(DIP)_2(mal)](PF_6)$** were investigated using cyclic voltammetry (CV) and rotating disc electrode (RDE) voltammetry. The RDE voltammogram (Figure S2) displays three well-defined wave features, in addition to that of decamethylferrocene used as internal reference and located at +0.090 V *vs* SCE. These electrochemical features are characterized by the same current intensity, which attests that the related redox processes involve the same number of electron transitions

(in this case one-electron transition). CV experiment (Figure S2) showed the complete reversibility of the redox processes. The redox potentials were assigned by comparison with the data reported in our recent paper on **[Ru(DIP)$_2$(sq)](PF$_6$)** (Table S1).[17] The process taking place at more positive potentials (+0.566 V *vs* SCE) can be attributed to the Ru(II)→Ru(III) oxidation, while the two processes at negative potentials can be assigned to the reduction of the ancillary ligands (DIP$^{0/-}$).[54],[55] The potential associated to the metal oxidation of **[Ru(DIP)$_2$(mal)](PF$_6$)** is almost 100 mV lower than what was observed for **[Ru(DIP)$_2$(sq)](PF$_6$)** in accordance with the higher electron donating property of the maltolate when compared to the semiquinonate ligand. No redox process involving the maltol appears in the potential range investigated, which is completely in agreement with the literature data.[56]

Solubility and Stability Studies in Different Solvents and Interaction with Human Serum Albumin

The biological ability of a compound is strongly influenced by its solution stability. The stability of **[Ru(DIP)$_2$(mal)](PF$_6$)** was first assessed in DMSO-d$_6$ using ^{1}H NMR spectroscopy since this solvent was found to be possibly problematic during biological experiments.[57]–[59] The ^{1}H NMR spectrum of **[Ru(DIP)$_2$(mal)](PF$_6$)** remained unchanged over 42 h at room temperature, revealing the stability of the complex in DMSO (Figure S3).

[Ru(DIP)$_2$(mal)](PF$_6$) shows limited solubility in water and in buffered aqueous media like 20 mM phosphate or HEPES buffer at pH 7.40. Dilution of ethanolic stock solutions of the complex in phosphate or HEPES buffer (≤ 2% (v/v) ethanol, 20 μM complex) afforded a precipitate after 1 h and 2 h, respectively, while dilution in water (pH ~ 8) afforded solutions that were stable at least for 6 h (Figure S4). It is important

to note that in no case decomposition of the complex (i.e. release of maltol) could be detected based on the UV-vis and ultrafiltration studies. Only the different rates of precipitation were observed by varying the type of the media (see more details in the SI, sections S5 and S7). Gradual aggregation followed by precipitation of the complex in buffered samples was seen. *In vitro* biological studies are usually performed in cell culture medium complemented with foetal calf serum (containing albumin as most abundant protein), hence, information about the solubility of the compound in these conditions is required. It was found that RPMI 1640 cell culture medium (non-complemented) could not hinder the precipitation of the complex (Figure S6/A). Therefore, interaction with the most abundant serum protein, albumin, was further investigated. In order to assay the albumin binding, samples were prepared both in phosphate and HEPES buffers (20 mM, $c_{complex}$ = 13.8 μM; 2% ethanol (v/v); pH = 7.40; T = 25 °C) with a protein-to-metal complex ratio of 6:1. The presence of the protein prevents precipitation of the metal complex in both media (Figure S6/B) confirming the binding interaction between human serum albumin (HSA) and **[Ru(DIP)$_2$(mal)](PF$_6$)**. The binding to the protein seems to take place via intermolecular bonding, since no release of maltol or 4,7-diphenyl-1,10-phenantroline could be detected by UV-vis spectroscopy in ultrafiltration experiments (Figure S7). HSA possesses hydrophobic binding pockets to accommodate small molecules, and binding at sites I and II of HSA was investigated spectrofluorimetrically due to the available site marker probe molecules (see details in Section S7). Interaction at site I was studied via the standard approach, namely following the quenching of the single Trp amino acid of HSA.[60] Determination of binding data was hindered by the complete overlapping of the weak intrinsic fluorescence of the metal complex with the protein Trp emission band (see Figure S8). The measured intensity upon the addition of the

complex to the protein is not the sum of the intensities of the complex and HSA (thus not additive), which indicates the binding interaction at site I and an upper limit of binding constant logK' < 4.0 could be estimated at this site.

Binding at site II was followed via site marker displacement experiment using dansylglycine (DG) as marker. DG was gradually displaced by **[Ru(DIP)$_2$(mal)](PF$_6$)** at site II (Figure 2). Calculated binding constant logK' (site II) = 4.3 ± 0.1 reveals moderate-to-weak binding affinity of **[Ru(DIP)$_2$(mal)](PF$_6$)** at site II.

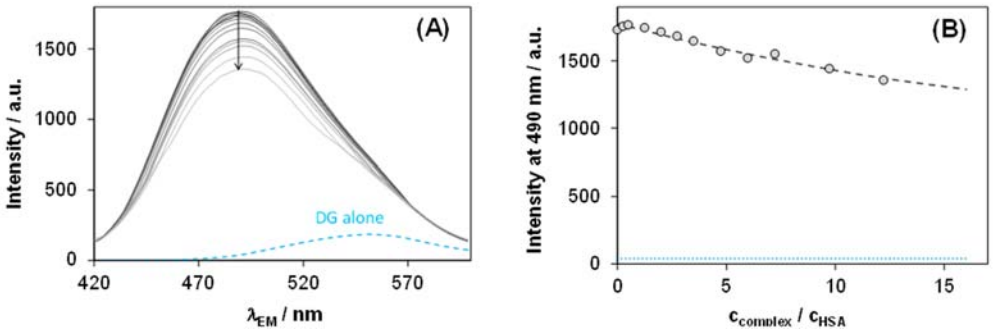

Figure 2. Fluorescence emission spectra obtained by the titration of HSA–DG (1:1) with **[Ru(DIP)$_2$(mal)](PF$_6$)** (A); and measured (dots) and calculated (dashed line) intensity values at 490 nm (B). Blue dotted line denotes the emission of free DG. {c_{HSA} = c_{DG} 2 μM; c_{comp} = 0–24 μM; λ_{EX} = 335 nm; pH = 7.40 (20 mM phosphate buffer); < 2% ethanol; T = 25 C}.

All in all, according to our results **[Ru(DIP)$_2$(mal)](PF$_6$)** binds to HSA via intermolecular interactions at least at the two hydrophobic sites: I and II. Albumin binding prevents precipitation of the metal complex in aqueous solution.

Stability Studies in Human Plasma

Next, to assess the behaviour of **[Ru(DIP)$_2$(mal)](PF$_6$)** under physiological conditions, its stability in human plasma was investigated by Ultra Performance Liquid Chromatography (UPLC) following a procedure already established by our group.[61]

[Ru(DIP)$_2$(mal)](PF$_6$) (0.12 mM) was incubated in human plasma up to 96 h at 37°C using caffeine (1.92 mM) as an internal standard.[62] The UV traces of the UPLC analysis at different incubation times are shown in Figure S9a. When the concentration of **[Ru(DIP)$_2$(mal)](PF$_6$)** was normalized with respect to the internal standard and plotted against time (Figure S9b), no clear decomposition was observed in the first 24 h, whereas a linear decrease in concentration started thereafter. Based on these changes the half-life of **[Ru(DIP)$_2$(mal)](PF$_6$)** could be estimated to be of approximately 48 h under these conditions.

Cytotoxicity Studies and Cell Death Mechanism

After assessment of stability in solution, **[Ru(DIP)$_2$(mal)](PF$_6$)** biological activity was investigated. The first step was to evaluate the cytotoxicity in 2D cell culture models, comprising HeLa (human cervical adenocarcinoma), A2780 (human ovarian carcinoma), A2780 cis (human cisplatin resistant ovarian carcinoma), A2780 ADR (human doxorubicin resistant ovarian carcinoma), CT-26 (mouse colon adenocarcinoma), CT-26 LUC (mouse colon adenocarcinoma stably expressing luciferase) and RPE-1 (human normal retina pigmented epithelial) cell lines and using a fluorometric cell viability assay (single graphs available in Figures S10).[63] In this study, doxorubicin and cisplatin were tested in the same cell lines and used as positive controls.[64],[65] Cytotoxicity of the **RuCl$_2$(DIP)$_2$** precursor and maltol ligand were also determined as additional controls. IC$_{50}$ values of the tested compounds are reported in Table 1. The cytotoxicity of **[Ru(DIP)$_2$(mal)](PF$_6$)** was found very high and comparable to what previously observed for **[Ru(DIP)$_2$(sq)](PF$_6$)**[17] in all cell lines tested in this study. The IC$_{50}$ values obtained are in the high nanomolar concentration range with the exception of the one determined on the doxorubicin-resistant cell line

(IC_{50} = 2.86 μM). The **$RuCl_2(DIP)_2$** precursor displays much lower cytotoxicity, while maltol, as expected, is non-toxic.[34],[35] **$[Ru(DIP)_2(mal)](PF_6)$** exerts an overall activity comparable to doxorubicin in all cell lines tested. Interestingly, its cytotoxicity against the cisplatin-resistant cell line is more than 40 times higher than that of cisplatin (IC_{50} = 0.42 μM vs. 18.33 μM for **$[Ru(DIP)_2(mal)](PF_6)$** and cisplatin, respectively).

Table 1. IC_{50} values for **$[Ru(DIP)_2(mal)](PF_6)$**, cisplatin, doxorubicin, **$[Ru(DIP)_2(sq)](PF_6)$**, **$RuCl_2(DIP)_2$** and maltol in different cell lines (48 h).

IC_{50} (μM)	**HeLa**	**A2780**	**A2780 ADR**	**A2780 cis**	**CT-26**	**CT-26 LUC**	**RPE-1**
Cisplatin*	9.28 ± 0.20	4.00 ± 0.76	8.32 ± 0.71	18.33 ± 2.92	2.60 ± 0.18	2.42 ± 0.23	30.24 ± 5.11
Doxorubicin*	0.34 ± 0.02	0.19 ± 0.03	5.94 ± 0.58	0.54 ± 0.04	0.082 ± 0.003	0.18 ± 0.006	0.89 ± 0.17
$[Ru(DIP)_2(sq)](PF_6)$*	0.50 ± 0.01	0.67 ± 0.04	4.13 ± 0.2	0.45 ± 0.03	1.00 ± 0.03	1.51 ± 0.14	0.90 ± 0.04
$[Ru(DIP)_2(mal)](PF_6)$	0.45 ± 0.04	0.74 ± 0.05	2.86 ± 0.3	0.42 ± 0.01	0.61 ± 0.02	0.72 ± 0.07	0.86 ± 0.04
$RuCl_2(DIP)_2$*	15.03 ± 0.4	4.69 ± 0.14	78.27 ± 4.9	6.36 ± 0.57	9.20 ± 1.22	6.65 ± 0.5	3.13 ± 0.07
Maltol	74.01 ± 14.6	>100	>100	>100	>100	>100	>100

* Values taken from [[17]] We, however, note that these experiments were performed on the same days.

Due to the promising activity displayed by **$[Ru(DIP)_2(mal)](PF_6)$** in monolayer cell culture, a MCTS model was also investigated.[66] 3D cultured cells are recognised as important research tools for their ability to resemble the pathophysiologic environment of the tumor tissue and,[67]–[69] along with the 2D model system, they allow for a better estimation of *in vivo* antitumour efficacy of compounds.[66],[68] The cytotoxicity of **$[Ru(DIP)_2(mal)](PF_6)$**, its **$RuCl_2(DIP)_2$** precursor, **$[Ru(DIP)_2(sq)](PF_6)$**, and the maltol ligand were tested *via* a luminescent cell viability assay in HeLa MCTS (single graphs are availabe in Figure S11). Cisplatin and doxorubicin were also tested in the same conditions as positive controls (Figure S11).[59,60] The IC_{50} values of the tested

compounds are reported in Table 2. **[Ru(DIP)$_2$(mal)](PF$_6$)** preserves the high cyotoxicity observed in the monolayer model with an IC_{50} value more than 2 times lower than cisplatin or doxorubicin (IC_{50} ~ 17 μM, 47 μM and 39 μM respectively), and comparable to that of **[Ru(DIP)$_2$(sq)](PF$_6$)**. The **RuCl$_2$(DIP)$_2$** precursor showed a cytotoxicity comparable to cisplatin while the maltol ligand was proven to be non-toxic also in this model.

Table 2. IC_{50} values for **[Ru(DIP)$_2$(mal)](PF$_6$)**, cisplatin, doxorubicin, **RuCl$_2$(DIP)$_2$** and maltol in multicellular HeLa cancer cell spheroids.

IC_{50} (μM)	**Cisplatin***	**Doxorubicin***	**[Ru(DIP)$_2$(sq)](PF$_6$)***	**[Ru(DIP)$_2$(mal)](PF$_6$)**	**RuCl$_2$(DIP)$_2$***	**Maltol**
HeLa MCTS	46.49 ± 4.18	38.59 ± 0.43	14.11 ± 0.09	17.00 ± 0.73	59.84 ± 3.05	>100

* Values taken from [[17]]. Notably, these experiments were performed on the same days.

Next, the size of treated MCTS was studied to evaluate the time dependent effect of the **[Ru(DIP)$_2$(mal)](PF$_6$)**. Growth kinetics of treated spheroids was monitored by changes in spheroids diameter. Briefly 400 μm HeLa MCTS were treated with different concentrations of **[Ru(DIP)$_2$(mal)](PF$_6$)**, and their diameter was checked every three days (Figure 3). Of note, when the washing step was performed, half of the medium was removed and replaced with fresh one, diluting twice the quantity of the compound in each well. At all concentrations tested, **[Ru(DIP)$_2$(mal)](PF$_6$)** caused a significant decrease in the size of the spheroids. Strikingly, this effect was still dominant even after 13 days of treatment.

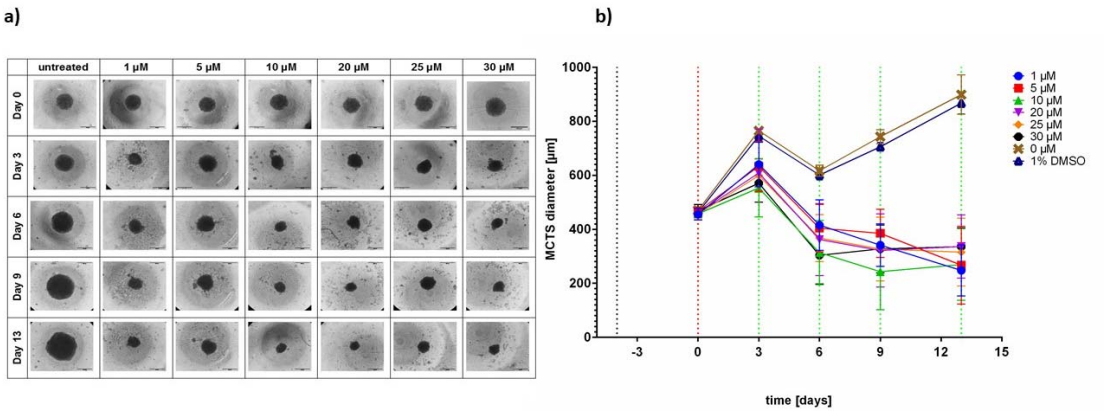

Figure 3. Changes in growth kinetics of MCTS treated with **[Ru(DIP)$_2$(mal)](PF$_6$)** at different concentrations (1, 5, 10, 20, 25 and 30 µM). (a) Images collected at day 0 (before treatment) and at day 3, 6, 9 and 13. b) MCTSs diameter measured at different time points. Blue-dotted line indicates the day of seeding, red-dotted line indicates the day of treatment while green-dotted lines indicate the days of washing.

In summary, **[Ru(DIP)$_2$(mal)](PF$_6$)** showed high cytotoxicity in 2D and 3D models, as well as prolonged effect on the spheroids growth. These promising results encouraged further evaluation of the mechanism of cell death caused by the complex. To determine whether cell death occurs by apoptosis or by necrosis process, HeLa cells were analysed by flow cytometry using the Annexin V and PI (propidium iodide) staining method. In this experiment, staurosporin, a known apoptosis inducer, was used as positive control.[72] 4 h incubation of HeLa cells with **[Ru(DIP)$_2$(mal)](PF$_6$)** (10 µM) induced considerable cell death, mostly through apoptosis. Longer incubation of the cells with the complex (24 h) significantly increased the number of cells undergoing apoptotic cell death. In comparison with staurosporin, only a small population of the cells was PI positive after 24 h treatment with **[Ru(DIP)$_2$(mal)](PF$_6$)**. Since PI is a vital stain (viable cells with intact membranes will exclude PI), this small population might refer either to dead cells or cells undergoing necrosis. Annexin V and PI staining confirmed that

[Ru(DIP)$_2$(mal)](PF$_6$) induces mostly apoptotic cell death in treated HeLa cells. Specific cell populations are shown in Figures 4 and S12.

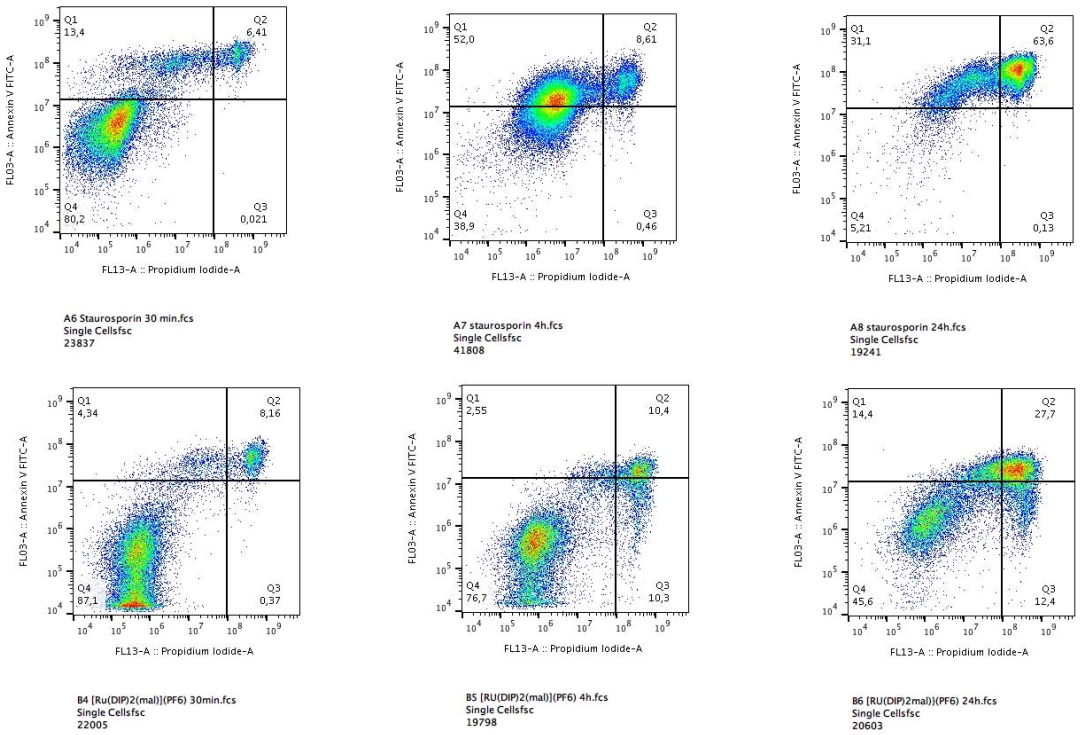

Figure 4. Annexin V and PI staining in HeLa cells treated with **[Ru(DIP)$_2$(mal)](PF$_6$)** (10 μM) and staurosporine (1 μM) at different time points. The fourth quadrant represents living cells (Annexin V, PI negative), first one early apoptotic cells (Annexin V positive, PI negative), second late apoptotic (Annexin and PI positive) and third necrotic or dead cells (Annexin V negative and PI positive).

Cellular Uptake, Biodistribution, and DNA Metalation.

To obtain more insights about the mode of action of **[Ru(DIP)$_2$(mal)](PF$_6$)**, it is essential to understand its cellular and subcellular accumulation as much as its mechanism of uptake. For this purpose, inductively coupled plasma mass spectrometry (ICP-MS) was utilised. Working concentrations and incubation times were chosen to avoid extended cell mass loss due to the high cytotoxicity of the complex but considering a ruthenium final amount that could allow determination of the metal

content. However, the working conditions (5 μM treatment for 2 h), in agreement with literature data, allowed for a minor accumulation of the drug cisplatin used as control.[73],[74] **[Ru(DIP)$_2$(mal)](PF$_6$)** accumulation in HeLa cells was found to be higher than its precursor and cisplatin used as controls and almost three times higher than the **[Ru(DIP)$_2$(sq)](PF$_6$)** analogue previously reported by our group (Figure 5a).[17] This could be explained by the different mechanism of cellular uptake associated to the two complexes. To fully understand the uptake mechanism, HeLa cells were pretreated or kept at different temperatures to determine if the uptake mechanism is passive or active. For this purpose, low temperature (4ºC should slow down passive diffusion as well as ATP required transport) or treatments with active transport inhibitors was utilised. 2-Deoxy-*D*-glucose and oligomycin block cellular metabolism (ATP production), chloroquine or NH_4Cl imped endocytic pathways and tetraethylammonium chloride stops cation transporters. After pre-treatment, cells were incubated with the compound (2 h, 5 μM) and subsequently analysed *via* ICP-MS (Figure S13). Inhibition of active uptake mechanisms did not perturb accumulation of **[Ru(DIP)$_2$(mal)](PF$_6$)** in HeLa cells. These findings clearly suggest that passive transport is the only mechanism responsible for accumulation of **[Ru(DIP)$_2$(mal)](PF$_6$)** in HeLa cells, unlike **[Ru(DIP)$_2$(sq)](PF$_6$)**, whose mechanism of uptake involves both active and passive transports.[17] Cellular fractionation experiments revealed the relative distribution of **[Ru(DIP)$_2$(mal)](PF$_6$)** among the different subcellular compartments (Figure 5b). Most of the complex was found in the cytoplasm, with mitochondria and lysosomes being the next most enriched organelles, while a smaller fraction was detected in the nucleus. **[Ru(DIP)$_2$(sq)](PF$_6$),** on the other hand, accumulated preferentially in the nucleus and only to a small extent in mitochondria,

lysosomes and cytoplasm.[17] The accumulation of a compound in the nucleus suggests DNA as one of the potential targets.

Even though only a small amount of ruthenium was found in the nucleus, the reactivity of our compound towards DNA was studied *via* DNA metalation experiment. HeLa cells were treated for 2 h with 5 µM solutions of **[Ru(DIP)$_2$(mal)](PF$_6$)** or cisplatin (positive control). The genetic material was then extracted, and the amount of metal was determined by ICP-MS. Data are shown in Figure 5c in comparison to those obtained for the analogue **[Ru(DIP)$_2$(sq)](PF$_6$)**.[17] These data point to a significant interaction between DNA and **[Ru(DIP)$_2$(mal)](PF$_6$)**, regardless of the small accumulation detected in the nucleus. The relative higher amount of metalated DNA found for **[Ru(DIP)$_2$(mal)](PF$_6$)** when compared to cisplatin or **[Ru(DIP)$_2$(sq)](PF$_6$)**, and upon normalization to total DNA, can be explained by the overall higher cellular uptake of the former complex.

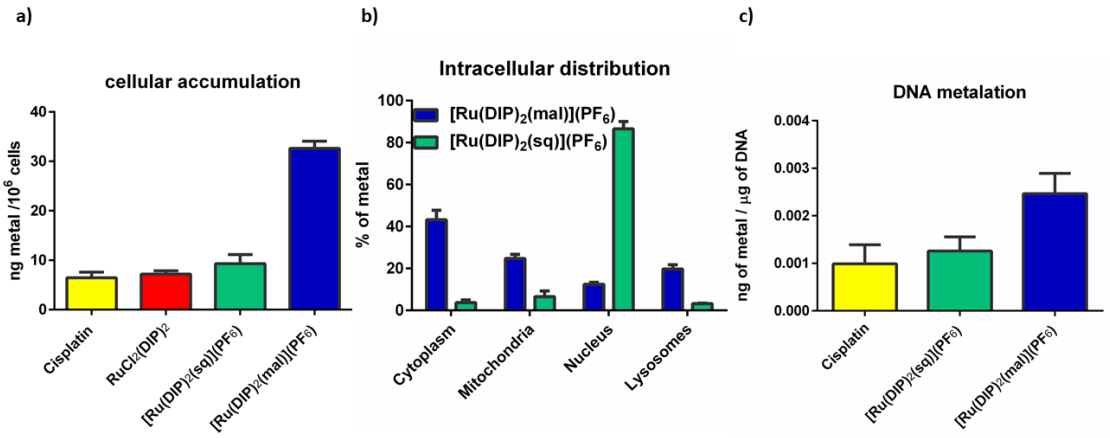

Figure 5. Cellular uptake (a), cellular fractionation (b) and DNA metalation (c) of HeLa cells after treatment with tested compounds (5 µM, 2 h). Data are presented as the mean ± SD of at least 3 technical replicates. All data related to **[Ru(DIP)$_2$(sq)](PF$_6$)** were previously reported by our group.[17] We, however, note that these experiments were performed on the same days.

JC-1 Mitochondrial Membrane Potential Test and Metabolic Studies.

The accumulation of **[Ru(DIP)$_2$(mal)](PF$_6$)** in mitochondria suggested studies on possible effects of the compound on mitochondrial function. To this end, we used JC-1, a green fluorescent monomer at low mitochondrial membrane potential (MMP) that aggregates and emits red fluorescence at higher potential.[75] MMP is a key factor of the mitochondrial function due to its direct correlation to oxidative phosphorylation.[76] Figure 6a shows the red fluorescence signal observed in HeLa cells upon 24 h treatment with **[Ru(DIP)$_2$(mal)](PF$_6$)**, FCCP (carbonyl cyanide 4-(trifluoromethoxy)phenylhydrazone, an uncoupling agent used as positive control),[77] and DMSO (vehicle control). An uncoupling agent is a molecule that inhibits the coupling between reactions of ATP synthesis and the electron transport chain leading to a disruption of oxidative phosphorylation in mitochondria.[78] Untreated cells are shown as a negative control. A significant concentration-dependent decrease in the fluorescence signal was observed upon treatment with **[Ru(DIP)$_2$(mal)](PF$_6$)** (from 0.1 μM to 0.6 μM). At the IC_{50} value (0.5 μM, marked in red in Figure 6a), the MMP decrease was comparable to that obtained for the positive control. However, it is important to take into consideration that a dramatic drop in MMP could be triggered by ongoing apoptosis.[77] These findings strongly suggest a contribution of impaired MMP to the cell death mechanism and inspired further studies on mitochondrial metabolism (i.e. oxidative phosphorylation) in HeLa cells. For this purpose, the Mito stress test was performed using Seahorse XF Analyzer. The low basal respiration observed in cells treated with **[Ru(DIP)$_2$(mal)](PF$_6$)** in comparison to untreated cells, clearly demonstrates a severe impairment of mitochondrial respiration. In contrast, the **RuCl$_2$(DIP)$_2$** precursor and the maltol ligand did not remarkably affect this process. Additionally, **[Ru(DIP)$_2$(mal)](PF$_6$)** caused a loss in the capacity of the mitochondrial membrane to restore the proton balance when treated with an uncoupling agent (FCCP)

and inhibited ATP production (Figure 6b and Figure S14). Taken together, these data demonstrate that **[Ru(DIP)$_2$(mal)](PF$_6$)** treatment causes complete disruption of mitochondrial respiration in HeLa cells. Furthermore, we investigated effects on other metabolic pathways, such as glycolysis, and the possible metabolic modulation of the three primary fuel pathways (involving glucose, glutamine or fatty acids as substrates) using a Seahorse XF Analyzer. The cytosolic process of glycolysis was not affected by **[Ru(DIP)$_2$(mal)](PF$_6$)** or its precursor (Figure S15). Effects on three primary fuel pathways could not be determined due to very low oxygen consumption rate in cells treated with **[Ru(DIP)$_2$(mal)](PF$_6$)** (Figure S16). Metabolic studies pointed to a substantial difference in the mode of action of **[Ru(DIP)$_2$(mal)](PF$_6$)** and the chemotherapeutic drug cisplatin. The latter is known to interfere with DNA replication and does not affect mitochondrial metabolism. **[Ru(DIP)$_2$(mal)](PF$_6$)**, on the other hand, clearly demonstrated that the mitochondrial disfunction is significantly involved in its mode of action.

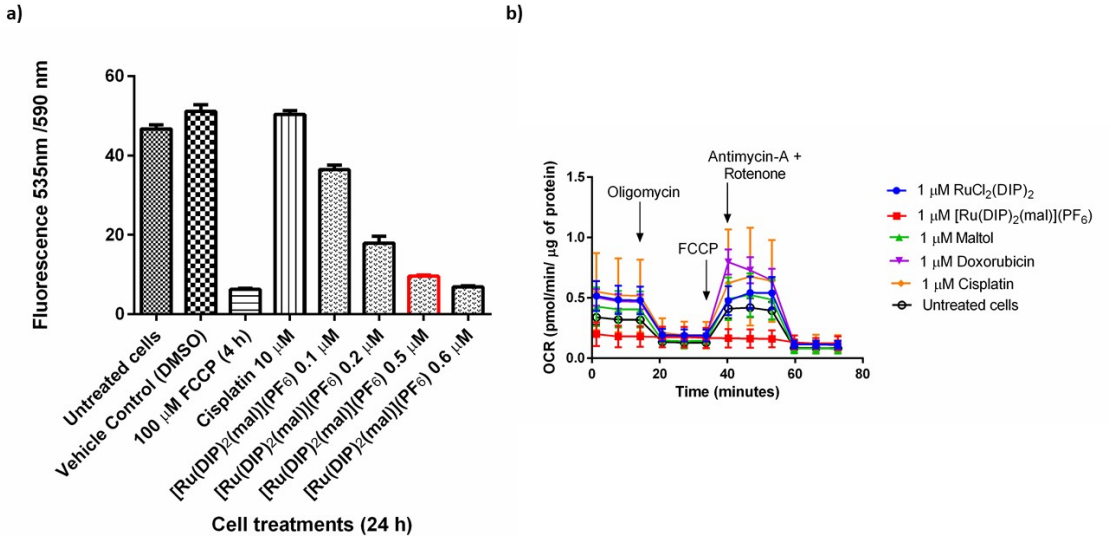

Figure 6. a) Fluorescence signal of JC-1 dye detected in HeLa cells treated for 24 h with different concentrations of **[Ru(DIP)$_2$(mal)](PF$_6$)** (from 0.1 μM to 0.6 μM). The bar marked in red indicates the IC$_{50}$ concentration (0.5 μM). FCCP was used as positive control, cisplatin and DMSO (1%) were used as negative controls. b) Mito Stress Test

profile after 24 h treatment; the graph displays oxygen consumption rate changes after treatment with specific electron transport chain inhibitors. Oligomycin (inhibitor of ATP synthase (complex V)), FCCP (uncoupling agent), Antimycin-A (complex III inhibitor) and Rotenone (complex I inhibitor).

Conclusions

Following the development of the potential anticancer agent **[Ru(DIP)$_2$(sq)](PF$_6$)** by our group, here we report synthesis and biological evaluation of an analogue complex, namely **[Ru(DIP)$_2$(mal)](PF$_6$)**, containing the FDA-approved, flavour-enhancing agent, maltol. It was found that the compound is stable at room temperature in DMSO over 42 h and has an half-life of 48 h in human plasma. Although the complex exhibits poor water solubility, the measurements in human plasma as well as in supplemented media were made possible by the presence of human serum albumin. In the course of this study, we demonstrated that **[Ru(DIP)$_2$(mal)](PF$_6$)** binds to HSA via intermolecular interactions at least at the two hydrophobic sites (I and II), preventing precipitation of the metal complex in aqueous solution. Studies performed on several cancerous cell lines in cellular monolayer culture and on HeLa MCTS indicated remarkable activity by **[Ru(DIP)$_2$(mal)](PF$_6$)**, comparable to doxorubicin and much higher than the approved drug cisplatin. It is worth nothing that **[Ru(DIP)$_2$(mal)](PF$_6$)** cytotoxicity against the cisplatin-resistant cell line is more than 40 times higher than that of cisplatin (IC_{50} = 0.42 μM vs. 18.33 μM for **[Ru(DIP)$_2$(mal)](PF$_6$)** and cisplatin, respectively) in 2D model cultures. Moreover, HeLa MCTS treated with different concentrations of **[Ru(DIP)$_2$(mal)](PF$_6$)** demonstrated a significant decrease in size, even after 13 days of a single treatment. Cellular uptake studies showed efficient cellular accumulation of the compound, when compared to cisplatin or the analogue **[Ru(DIP)$_2$(sq)](PF$_6$)**, through a passive transport mechanism. Deeper investigations on **[Ru(DIP)$_2$(mal)](PF$_6$)** mode of action by means of cellular fractionation, showed

mitochondria as one of the preferred accumulation sites. Mitochondrial disfunction was assessed through a mito-stress test (Seahorse technology) and changes in MMP (JC-1 staining): both approaches led to establish a conclusive contribution of impaired mitochondria metabolism in the mode of action of **[Ru(DIP)$_2$(mal)](PF$_6$)**. Finally, metalation studies confirmed the interaction between **[Ru(DIP)$_2$(mal)](PF$_6$)** and DNA, suggesting the latter as another potential target. These findings together with what previously reported on the activity of **[Ru(DIP)$_2$(sq)](PF$_6$)**, emphasise the outstanding potential of this class of compounds, which should be taken into account from scientists involved in the search of new chemotherapeutic agents.

Experimental Section

Materials.

All chemicals were either of reagent or analytical grade and used as purchased from commercial sources without additional purification. $RuCl_3$ hydrate was provided by I^2CNS, 4,7-Diphenyl-1,10-phenanthroline, LiCl (anhydrous, 99%), and maltol by Alfa Aesar, tetrabutylammonium hexafluorophosphate by Sigma-Aldrich. All solvents were purchased of analytical, or HPLC grade. When necessary, solvents were degassed by purging with dry, oxygen-free nitrogen for at least 30 min before use.

Instrumentation and methods.

Amber glass or clear glassware wrapped in tin foil was used when protection from light was necessary. Schlenk glassware and a vacuum line were employed when reactions sensitive to moisture/oxygen had to be performed under nitrogen atmosphere. Thin layer chromatography (TLC) was performed using silica gel 60 F-254 (Merck) plates with detection of spots being achieved by exposure to UV light. Column chromatography was done using Silica gel 60-200 μm (VWR). Eluent mixtures are expressed as volume to volume (v/v) ratios. ^1H and ^{13}C NMR spectra were measured on Bruker Avance III HD 400 MHz or Bruker Avance Neo 500 MHz spectrometers using the signal of the deuterated solvent as an internal standard.[79] The chemical shifts (δ) are reported in ppm (parts per million) relative to tetramethylsilane (TMS) or signals from the residual protons of deuterated solvents. Coupling constants J are given in Hertz (Hz). The abbreviation for the peaks multiplicity is s (singlet), d (doublet), dd (doublet of doublet), m (multiplet). ESI-HRMS experiments were carried out using a LTQ-Orbitrap XL from Thermo Scientific (Thermo Fisher Scientific, Courtaboeuf, France) and operated in positive ionization mode, with a spray voltage at 3.6 kV. Sheath and auxiliary gas were set at a flow rate of 5 and 0 arbitrary units (a.u.), respectively.

The voltages applied were 40 and 100 V for the ion transfer capillary and the tube lens, respectively. The ion transfer capillary was held at 275°C. Detection was achieved in the Orbitrap with a resolution set to 100,000 (at m/z 400) and a m/z range between 200-2000 in profile mode. Spectrum was analysed using the acquisition software XCalibur 2.1 (Thermo Fisher Scientific, Courtaboeuf, France). The automatic gain control (AGC) allowed accumulation of up to 2.105 ions for FTMS scans, Maximum injection time was set to 300 ms and 1 μscan was acquired. 5 μL was injected using a Thermo Finnigan Surveyor HPLC system (Thermo Fisher Scientific, Courtaboeuf, France) with a continuous infusion of methanol at 100 $\mu L min^{-1}$. Elemental analysis was performed at Science Centre, London Metropolitan University using Thermo Fisher (Carlo Erba) Flash 2000 Elemental Analyser, configured for %CHN. IR spectra were recorded with SpectrumTwo FTIR Spectrometer (Perkin–Elmer) equipped with a Specac Golden GateTM ATR (attenuated total reflection) accessory; applied as neat samples; $1/\lambda$ in cm^{-1}. Stability in human plasma was performed on HPLC (VWR Hitachi Chromaster system) and a Macherey Nager EC 250/3 Nucleosil 100-5 C18 column. UV absorption was measured at 275 nm and the runs (flow rate 0.6 $mL min^{-1}$) were performed with a linear gradient of A (distilled water containing 0.1% (v/v) TFA) and B (acetonitrile, Sigma-Aldrich HPLC grade): t = 0 min, 5% B; t = 0.5 min, 5% B; t = 1.5 min, 100% B; t = 2 min, 100% B. Ruthenation of the DNA was performed using a High-Resolution ICP-MS Element II from ThermoScientific located within the Environmental Biogeochemistry team of the Institut de Physique du Globe de Paris. This ICP-MS enables working in different resolution modes (LR=400, MR=4000 and HR=10000) for a better discrimination between elements of interest and interferences.[80] For the metabolic studies Seahorse XFe96 Analyser by Agilent Technologies was used.

$RuCl_2(DMSO)_4$ was synthesised following an adapted literature procedure.[52] Spectroscopic data (^{1}H NMR) was in agreement with literature.[52]

Synthesis and characterization.

$Ru(DIP)_2Cl_2$. The complex was synthesised following an adapted literature procedure.[53] A mixture of $RuCl_2(DMSO)_4$ (3.0 g, 6.19 mmol), 4,7-diphenyl-1,10-phenanthroline (DIP, 4.11 g, 12.38 mmol) and LiCl (2.0 g, 47.18 mmol) dissolved in DMF (100 mL) was refluxed for 24 h. After cooling to *r.t.* the solvent was reduced *in vacuo* to 8 mL and 350 mL of acetone were added. After overnight storage at -20 °C the deep purple solid was removed by filtration with a Buchner funnel and washed with cold acetone and Et_2O. $Ru(DIP)_2Cl_2$ was then collected, dried and purified by silica gel chromatography (DCM/MeOH 97:3 *rf* 0.4) to afford the complex in 52% yield (2.71 g, 3.23 mmol,) which purity was confirmed by microanalysis. Spectroscopic data (^{1}H NMR) were in agreement with literature.[53]

$[Ru(DIP)_2(mal)](PF_6)$

$Ru(DIP)_2Cl_2$ (0.150 g, 0.18 mmol) and aq. NaOH (0.28 mL, 1 M) were dissolved in ethanol (18 mL). The solution was degassed for 30 min and maltol (3-Hydroxy-2-methyl-4H-pyran-4-one) (0.036 g, 0.29 mmol) was added. The mixture was heated to reflux for 3 h under N_2 atmosphere and protected from light. After cooling to r.t., H_2O (200 mL) and NH_4PF_6 (1 g, 6 mmol) were added. The mixture was stored overnight in the refrigerator (4 °C). The precipitate was collected on a Buchner funnel, washed with H_2O (3 × 50 mL) and Et_2O (3 × 50 mL). The solid was sonicated with Et_2O or Heptane (10 mL) for 10 min and then centrifuged. This procedure was repeated three times for each solvent. The solid was eventually dried under vacuum to deliver a clean product as the PF_6 salt (0.17 g, 0.16 mmol, 90%). IR (Golden Gate, cm^{-1}): 1590w, 1545w,

1490w, 1465w, 1445w, 1415w, 1400w, 1275w, 1205w, 1085w, 1025w, 915w, 830s, 765s, 735m, 700s. ^{1}H NMR (400 MHz, CD_2Cl_2): δ/ppm = 9.49 (d, J = 5.4 Hz, 1H), 9.33 (d, J = 5.5 Hz, 1H), 8.23 (dd, J = 9.4, 4.6 Hz, 2H), 8.13 (dd, J = 9.4, 1.1 Hz, 2H), 8.04 (d, J = 5.6 Hz, 2H), 7.98 (dd, J = 13.5, 5.4 Hz, 2H), 7.78 – 7.60 (m, 11H), 7.59 – 7.47 (m, 10H), 7.33 (dd, J = 5.6, 3.0 Hz, 2H), 6.54 (d, J = 5.1 Hz, 1H), 2.37 (s, 3H). ^{13}C NMR (125 MHz, CD_2Cl_3): δ/ppm = 185.00, 159.02, 155.49, 154.10, 154.01, 151.75, 151.47, 151.06, 150.64, 150.17, 149.98, 149.92, 147.66, 147.13, 146.01, 145.71, 136.50, 136.47, 136.23, 136.20, 130.15, 129.86, 129.81, 129.47, 129.44, 129.28, 129.21, 129.10, 128.78, 128.61, 128.55, 128.46, 125.96, 125.82, 125.77, 125.77, 125.69, 125.51, 125.25, 125.05, 112.40, 29.84. HRMS (ESI+): m/z 891.19042 $[M - PF_6]^+$. Elemental Analysis: calcd. for $C_{54}H_{39}F_6N_4O_4PRu$ = C, 61.54; H, 3.73; N, 5.32. Found = C, 61.53; H, 3.38; N, 5.17.

Electrochemical Measurements.

Electrochemical experiments were carried out with a conventional three-electrodes cell (solution volume of 15 mL) and a PC-controlled potentiostat/galvanostat (Princeton Applied Research Inc. model 263A). The working electrode was a vitreous carbon electrode from Origalys (France) exposing a geometrical area of 0.071 cm^2 and mounted in Teflon®. The electrode was polished before each experiment with 3 and 0.3 μm alumina pastes followed by extensive rinsing with ultra-pure Milli-Q water. A platinum wire was used as counter electrode and saturated calomel electrode, SCE, as reference electrode. Electrolytic solutions, DMF containing tetrabutylammonium hexafluoroborate 0.1M ($TBAPF_6$, Aldrich, +99 %) as supporting electrolyte, were routinely deoxygenated by argon bubbling. All the potential values are given versus the calomel saturated electrode SCE and recalculated versus $Me_{10}Fc^{0/+}$ potential value.

DMSO and Human Plasma stability studies.

The stability in DMSO-d_6 at room temperature was assessed by ^{1}H NMR over 42 hours. The stability of the complex in human plasma at 37 °C was evaluated following an adapted procedure recently reported by our group.[81] Human plasma was provided by the Blutspendezentrum, Zurich, Switzerland. Caffeine was obtained from Sigma-Aldrich and used as an internal standard.[62] Stock solutions of the complex (9.6 mM) in DMSO and caffeine (0.15 M) in H_2O were prepared. For a typical experiment, an aliquot of 12.5 µL of each stock solution was added to the plasma solution (975 µL) to a total volume of 1000 µL and final concentration of 1.92 mM for caffeine and 0.12 mM for the complex. The resulting plasma solution was incubated for 0, 1, 2, 4, 6, 24, 48, 72 and 96 h at 37 °C with continuous and gentle shaking (ca. 600 rpm). The reaction was stopped by addition of 2 mL of MeOH, and the mixture was centrifuged for 45 min at 3500 rpm. The methanolic solution was filtered and analysed using HPLC and an injection volume of 6 µL.

Stability of the complex in different solvents and at different conditions.

Preparation of stock solutions: Human serum albumin (HSA as lyophilized powder with fatty acids), Na_2HPO_4, NaH_2PO_4, 4-(2-hydroxyethyl)-1-piperazineethanesulfonic acid (HEPES) and danysylglycine (DG) were obtained from Sigma-Aldrich in *puriss* quality. Powdered RPMI 1640 cell culture medium without indicator for 1 L solution was a Sigma-Aldrich product as well. Milli-Q ultrapure water was used for sample preparations. HSA solution was freshly prepared before the experiments in 20 mM phosphate or in 20 mM HEPES buffer (pH = 7.40). Its concentration was estimated

from its UV absorption: $\varepsilon_{280\ nm}$(HSA) = 36850 $M^{-1}cm^{-1}$.[82] Stock solutions of the complex were freshly prepared every day in ethanol in 1-2 mM concentration.

^{1}H NMR measurements: ^{1}H NMR spectroscopic studies were carried out on a Bruker Avance III HD Ascend 500 Plus instrument. The metal complex was dissolved in methanol-d^4 in 3.3 mM concentration. Samples prepared in methanol-d^4, RPMI 1640 medium or in 20 mM phosphate buffer (pH = 7.40) contained 1 mM metal complex and 30% (v/v) methanol-d^4. Spectra for water containing samples were recorded with the WATERGATE water suppression pulse scheme using DSS internal standard.

UV-Vis spectrophotometry and ultrafiltration: An Agilent Carry 8454 diode array spectrophotometer was utilized to record the UV–visible (UV–vis) spectra in the interval 190–1100 nm. The path length (l) was 1 cm. Aqueous stability of the complex was followed in 20 mM phosphate buffer (pH = 7.40), in 20 mM HEPES buffer (pH = 7.40), in RPMI 1640 medium, in the presence of HSA, in ethanol, methanol and in pure water (pH ~ 8). Measurements on the protein binding of the complex were performed at fixed metal complex concentration (20 μM) and various protein-to-complex ratios (from 0.02:1 to 10:1) were applied.

Spectrofluorometric studies: Samples were prepared in 20 mM phosphate or in 20 mM HEPES buffer (pH 7.40); spectra were recorded after 5 min incubation. Samples for quenching experiments contained 1 μM HSA and various HSA-to-metal complex ratios (from 1:0 to 1:15) were used. The excitation wavelength was 295 nm; the emission intensities were read in the range of 305 – 500 nm with 5 nm/5 nm slit widths. In the site marker displacement experiments, the HSA-to-DG ratio was 1:1 (2-2 μM) and the concentration of the metal complex was varied from 0 to 37 μM. The excitation wavelength was 335 nm and the emission intensity was collected in the range of 420 – 600 nm with 5 nm/10 nm slit widths. The conditional binding constant for the site II

binding of the complex was calculated with the computer program HypSpec[83] as described in our previous works.[29],[84] Corrections for self-absorbance and inner filter effect were done.[60]

Cell culture.

HeLa and CT-26 cell lines were grown in DMEM media (Gibco). CT-26 LUC cell line was cultured in DMEM media (Gibco) supplemented with 1.6 mg/mL of Genticin. RPE-1 cell line was grown and maintained in DMEM/F-12 media (Gibco). A2780, A2780 cis, A2780 ADR cell lines were cultured in RPMI 1640 media (Gibco). The resistance of A2780 cis was maintained by cisplatin treatment (1μM) for one week every month. Cells were used in the assays one week after the end of the treatment, in order to avoid interferring results. The resistance of A2780 ADR was maintained by doxorubicin treatment (0.1 μM) once a week. Cells were used in the assays after three days post doxorubicin treatment in order to avoid interferring results. All cell lines were complemented with 10% of fetal calf serum (Gibco) and 100 U/mL penicillin-streptomycin mixture (Gibco) and maintained in humidified atmosphere at 37°C and 5% of CO_2.

Cytotoxicity Assay using a 2D cellular model.

Cytotoxicity of **$[Ru(DIP)_2(mal)](PF_6)$** and **$RuCl_2(DIP)_2$** complexes was assessed by a fluorometric cell viability assay using Resazurin (ACROS Organics). Briefly, cells were seeded in triplicates in 96-well plates at a density of 4×10^3 cells/well in 100 μL. After 24 h, cells were treated with increasing concentrations of the ruthenium complexes. Dilutions for **$[Ru(DIP)_2(mal)](PF_6)$** and **$RuCl_2(DIP)_2$** were prepared as follows: 2.5 mM stock in DMSO (**$[Ru(DIP)_2(mal)](PF_6)$**) or DMF (**$RuCl_2(DIP)_2$**) was

prepared, which was further diluted to 100 µM and filtered (0.22 µm filter VWR). After 48 h incubation, the medium was removed and 100 µL of complete medium containing resazurin (0.2 mg/mL final concentration) was added. After 4 h of incubation at 37 °C, the fluorescence signal of resorufin product was read (ex: 540 nm em: 590 nm) in a SpectraMax M5 microplate Reader. IC_{50} values were then calculated using GraphPad Prism software.

Generation of 3D HeLa MCTS.

MCTS were cultured using ultra-low attachment 96 wells plates from Corning® (Fisher Scientific 15329740). HeLa cells were seeded at a density of 5000 cells per well in 200 µL medium. The single cells would generate MCTS approximately 400 µm in diameter at day 4 with 37 °C and 5 % CO_2.

Treatment of 3D HeLa MCTS.

After 4 days of growing at 37 °C and 5% CO_2, HeLa MCTS were treated for 48 h by replacing half of the medium in the well with medium containing increasing concentration of compounds. For untreated reference MCTS, half of the medium was replaced by fresh medium only. Cytotoxicity was measured by quantification of ATP concentration with CellTiter-Glo® Cell viability kit (Promega, USA).

HeLa MCTSs growth inhibition.

MCTSs were grown and treated as described above. MCTSs sizes were observed under a light microscope and pictures were taken with an iPhone 6s thanks to a phone microscope adaptor. Before imaging, the plate was shaken, and half of the media was exchanged to remove dead cells. Images were recorded before treatment (day 0) and at

day 3, 6, 9 and 13 after treatment. Pictures were first processed using GIMP a cross-platform image editor with a batch automation plug-in. The MCTSs sizes were then calculated with SpheroidSizer, a MATLAB-based and open-source software application to measure the size of tumour spheroids automatically and accurately. Data analysis was done using GraphPad Prism software.

Annexin V / PI assay.

Apoptosis and necrosis induction in HeLa cells treated with **[Ru(DIP)$_2$(mal)](PF$_6$)** was evaluated *via* an AnnexinV/PI staining assay using flow cytometry. Briefly, cells were seeded at density of 2×10^6 cells in 10 cm cell culture dish 24 h prior cell treatments. The medium was removed and replaced with 10 μM solution of complex **[Ru(DIP)$_2$(mal)](PF$_6$)** or 1 μm Staurosporin (positive control -Abcam Cat no.120056) and further incubated for 30 min, 4 h or 24 h. Cells were collected, washed twice with ice cold PBS and resuspended in 1x Annexin V binding buffer (10 x buffer composition: 0,1 M HEPES (pH 7.4), 1.4 M NaCl. 25 mM $CaCl_2$). Samples were processed according to the manufacturer instructions (BD Scientific, cat no 556463 and 556419) and analysed using ZE5 Biorad instrument at Cytometry Platform at Institute Curie. Data were analysed using the FlowJo software.

Sample Preparation for cellular uptake.

Cells were seeded at density of 2×10^6. Next day, cells were treated with 5 μM concentration of **[Ru(DIP)$_2$(mal)](PF$_6$)** or **RuCl$_2$(DIP)$_2$**. After 2 h, cells were collected, counted and snap frozen in liquid nitrogen and stored at -20 ºC. ICP-MS samples were prepared as follows: samples were digested using 70% nitric acid (1 mL, 60 ºC, overnight). Samples were then further diluted 1:100 (1% HCl solution in MQ

water) and analysed using ICP-MS.

Sample Preparation for cellular fractionation.

HeLa cells were seeded in three 15 cm^2 cell culture dishes so that on the day of treatment cells were 90% confluent. On the day of treatment cells were incubated with the target complex at a concentration of 5 μM for 2 h. After that time, the medium was removed; cells were washed, collected and counted. After resuspension in cold PBS, the organelles were isolated via different protocols (one cell culture dish per isolation was used).

Mitochondria isolation: To isolate mitochondria, a Mitochondria Isolation Kit (Cat. Nr: MITOISO2, Sigma Aldrich) was used according to the manufacturer procedure for isolation of mitochondria *via* homogenization method.

Lysosome isolation: To isolate lysosomes, a Lysosome Isolation Kit (Cat. Nr: LYSISO1, Sigma Aldrich) was used, according to the manufacturer procedure for isolation of lysosomes *via* Option C.

Nuclear and cytoplasm isolation: To isolate nuclear and cytoplasmic fractions, the ROCKLAND nuclear extract protocol was used.[85] Briefly cells were collected by centrifugation, resuspended in cytoplasmic extraction buffer and incubated on ice. The tubes were centrifuged and supernatant (CE) was removed. Pellets were washed with cytoplasmic extraction buffer without detergent and centrifuged. The pellet (NE) was resuspended in nuclear extraction buffer and incubated on ice. Both CE and NE were centrifuged. Supernatant from CE samples was indicated as cytoplasmic extract, whereas the pellet obtained from NE samples was indicated as nuclear extract.

ICP-MS samples were prepared as follows: isolated cellular fractions were lyophilised and digested using 5 mL of 70% nitric acid (60 ºC, overnight). Samples were then

further diluted 1:200 –for nuclear pellet samples and 1:20 for all the other samples (1% HCl solution in MQ water) and analysed using ICP-MS.

Sample preparation for studies on the mechanism of cellular uptake

Samples were prepared as previously reported.[17] Briefly, HeLa cells were seeded at density of 2×10^6 and next day were pre-treated with corresponding inhibitors or kept at specific temperature for 1 h. Next, cells were washed with PBS and were incubated with 5 μM **[Ru(DIP)$_2$(mal)](PF$_6$)** for 2 h (low temperature sample was still kept at 4 ºC). Afterwards cells were washed with PBS, collected, counted and snap frozen in liquid nitrogen. Pellets were stored at -20 ºC. ICP-MS samples were prepared as follows: samples were digested using 70% nitric acid (1 mL, 60 ºC, overnight), further diluted 1:100 (1% HCl solution in MQ water) and analysed using ICP-MS.

DNA metalation of HeLa cells.

Cells were seeded at density of 2 x 10^6. The following day, cells were treated with 5 μM concentration of **[Ru(DIP)$_2$(mal)](PF$_6$)** or cisplatin. After 2 h, cells were collected, snap frozen in liquid nitrogen and stored at -20 ºC. The following day, DNA was extracted using a PureLink™ Genomic DNA Mini Kit (Invitrogen). DNA purity was checked by absorbance measurements at 260 and 280 nm. Concentrations of genomic DNA were calculated assuming that one absorbance unit equals 50 μg/mL. ICP-MS samples were prepared as follows: samples were digested using 70% nitric acid (60 ºC, overnight) in 1:1.6 DNA to acid volume ratio. Samples were then further diluted 1:10

or 1:100 (1% HCl solution in MQ water) and analysed using ICP-MS.

ICP-MS studies.

Daily, prior to the analytical sequence, the instrument was first tuned to produce maximum sensitivity and stability while also maintaining low uranium oxide formation (UO/U ≤ 5%). The data were treated as follow: intensities were converted into concentrations using uFREASI (user-FRiendly Elemental dAta proceSsIng).[86] This software, made for HR-ICP-MS users community, is free and available on http://www.ipgp.fr/~tharaud/uFREASI.

ICP-MS data analysis.

Cellular uptake studies: The amount of metal detected in the cell samples was transformed from ppb into µg of metal. Data were subsequently normalised to the number of cells and expressed as µmol of metal/ amount of cells.

Cellular fractionation: The amount of detected ruthenium in the cell samples was transformed from ppb into µg of ruthenium. Values were then normalised to the number of cells used for specific extraction. Due to low yield of lysosome extraction (only 25%), the values obtained were multiplied by the factor of 4. Because of a low yield of mitochondria extraction (50% of the cells were homogenized), the values obtained for that organelle were multiplied by the factor of 2. Extraction protocols allow for the isolation of pure subcellular fractions. Therefore, the total amount of metal found in the cells was calculated summing the values obtained for the pure organelles.

Mechanism of uptake: The amount of ruthenium detected in cell samples was transformed from ppb into µg of ruthenium and values obtained were normalised to the

number of cells used for specific treatment. The value for the ruthenium found in the 37 ºC sample was used as a 100%.

Cellular metalation: The amount of ruthenium detected in cell samples was transformed from ppb into µg of ruthenium and value obtained was normalised to the amount of DNA.

JC-1 Mitochondrial Membrane Potential Test.

HeLa cells were seeded at a density of 6000 cells / well in black 96 well-plates (Costar 3916). The following day, cells were treated with different concentrations of **[Ru(DIP)$_2$(mal)](PF$_6$)** and **RuCl$_2$(DIP)$_2$**. After further 24 h, cells were treated according to the instructions of the JC-1 Mitochondrial Membrane Potential Assay Kit (Abcam, ab113850). The data were analysed using GraphPad Prism software.

Metabolic Studies

HeLa cells were seeded in Seahorse XFe96 well plates at a density of 30,000 cells / well in 80 µL medium. After 24 h, the medium was replaced with fresh medium and cisplatin (1 µM), doxorubicin (1 µM), maltol (1 µM), complex **RuCl$_2$(DIP)$_2$** (1 µM) or complex **[Ru(DIP)$_2$(mal)](PF$_6$)** (1 µM) were added. After 24 h of incubation, the regular medium was removed, cells were washed thrice using Seahorse Base Media and incubated in a non-CO_2 incubator at 37 °C for 1 h.

Mito Stress Test: Mitostress assay was run using Oligomycin, 1 µM, FCCP 1 µM and mixture of Antimycin-A/ Rotenone 1 µM each in ports A, B and C respectively using Seahorse XFe96 Extracellular Flux Analyzer.

Glycolysis Stress Test: Glycolytic stress test was run using glucose (10 mM), Oligomycin (1 μM) and 2-Deoxyglucose (50 mM) in ports A, B and C respectively using Seahorse XFe96 Extracellular Flux Analyzer.

Mito Fuel Flex Test: Fuel flex assay for the different fuel pathways viz. glucose, glutamine and fatty acid was studied by measuring the basal oxygen consumption rates and that after addition of the inhibitor of the target pathway in port A and a mixture of the inhibitors of the other two pathways in port B. This gave a measure of the dependency of the cells on a fuel pathway. To study the capacity of a certain fuel pathway, the sequence of addition of the inhibitors was reversed. In port A was added the mixture of inhibitors for the other pathways and in port B was added the inhibitor for the target pathway. UK-5099 (pyruvate dehydrogenase inhibitor, 20 μM) was used as an inhibitor for the glucose pathway. BPTES (selective inhibitor of Glutaminase GLS1, 30 μM) was used as an inhibitor for the glutamine pathway. Etomoxir (O-carnitine palmitoyltransferase-1 (CPT-1) inhibitor, 40 μM) was used as an inhibitor for the fatty acid pathway.

Associated Content

Supporting Information

The Supporting Information is at DOI: XXXXX.

NMR spectra of **[Ru(DIP)$_2$(mal)](PF$_6$)** (Figure S1), voltammograms recorded by CV and with the use of RDE for **[Ru(DIP)$_2$(mal)](PF$_6$)** (Figure S2), electrochemical data for **[Ru(DIP)$_2$(mal)](PF$_6$)** (Table S1), overlap of ^{1}H spectra of **[Ru(DIP)$_2$(mal)](PF$_6$)** in DMSO-d^6 over 42h days (Figure S3), detailed investigation on the stability of the complex in different solvents and conditions (section 5, Figure S4, S5), RP-UPLC

traces of **[Ru(DIP)$_2$(mal)](PF$_6$)** (a) and percentage concentration of **[Ru(DIP)$_2$(mal)](PF$_6$)**, normalized with respect to the internal standard and plotted against time (b) (Figure S6), more details on interaction with human serum albumin (section S7, Figures S7-S9), fluorometric cell viability assay (Figure S10), CellTiter Glo® viability Test (Figure S11), Cell Death Mechanism (Figure S12) cellular uptake mechanism of **[Ru(DIP)$_2$(mal)](PF$_6$)** (Figure S13), oxygen consumption rates and different respiration parameters in HeLa cells alone or after treatment with various test compounds (Figure S14), extracellular acidification rate and different parameters during glycolysis in HeLa cells alone or after treatment with various test compounds (Figure S15), Fuel flex assay in HeLa cells (Figure S16).

Acknowledgements

This work was financially supported by an ERC Consolidator Grant PhotoMedMet to G.G. (GA 681679) and has received support under the program *Investissements d'Avenir* launched by the French Government and implemented by the ANR with the reference ANR-10-IDEX-0001-02 PSL (G.G.). This work was financed by the Swiss National Science Foundation (Professorships N° PP00P2_133568 and PP00P2_157545 to G.G.), the University of Zurich (G.G), the Novartis Jubilee Foundation (G.G. and R.R.), the Forschungskredit of the University of Zurich (R.R.), the University of Trieste (E.A., FRA 2018), and the UBS Promedica Stiftung (G.G. and R.R.). Ile de France Region is gratefully acknowledged for financial support of 500 MHz NMR spectrometer of Chimie-ParisTech in the framework of the SESAME equipment project. We acknowledge the loan of Agilent's equipment to Chimie ParisTech. This work was supported by National Research, Development and Innovation Office-

NKFIA through projects GINOP-2.3.2-15-2016-00038, FK 124240. SF is supported by the Czech Science Foundation grant 17-02080S.

Table of contents (TOC)

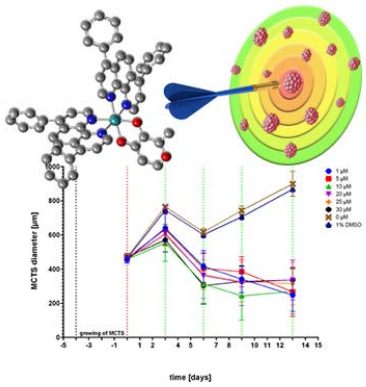

References.

[1] Gasser, G.; Ott, I.; Metzler-Nolte, N. *J. Med. Chem.* **2011**, *54*, 3–25.

[2] Rosenberg, B. B. *Platin. Met. Rev.* **1971**, *15*, 42–51.

[3] Wong, E.; Giandomenico, C. M. *Chem. Rev.* **1999**, *99*, 2451–2466.

[4] Antonarakis, E. S.; Emadi, A. *Cancer Chemother. Pharmacol.* **2010**, *66*, 1–9.

[5] Alessio, E. *Eur. J. Inorg. Chem.* **2017**, *55*, 1549–1560.

[6] Zeng, L.; Gupta, P.; Chen, Y.; Wang, E.; Ji, L.; Chao, H.; Chen, Z.-S.; Mai, J.; Zhang, H.; Li, Z.; et al. *Chem. Soc. Rev.* **2017**, *46*, 5771–5804.

[7] Alessio, E.; Messori, L. *Molecules* **2019**, *24*, 1995.

[8] Sava, G.; Capozzi, I.; Clerici, K.; Gagliardi, G.; Alessio, E.; Mestroni, G. *Clin. Exp. Metastasis* **1998**, *16*, 371–379.

[9] Lentz, F.; Drescher, A.; Lindauer, A.; Henke, M.; Hilger, R. a; Hartinger, C. G.; Scheulen, M. E.; Dittrich, C.; Keppler, B. K.; Jaehde, U. *Anticancer. Drugs* **2009**, *20*, 97–103.

[10] Trondl, R.; Heffeter, P.; Kowol, C. R.; Jakupec, M. a.; Berger, W.; Keppler, B. K. *Chem. Sci.* **2014**, *5*, 2925–2932.

[11] Hartinger, C. G.; Zorbas-Seifried, S.; Jakupec, M. A.; Kynast, B.; Zorbas, H.; Keppler, B. K. *J. Inorg. Biochem.* **2006**, *100*, 891–904.

[12] Yin, H.; Roque, J.; Konda, P.; Monro, S.; Colo, K. L.; Gujar, S.; Thummel, R. P.; Lilge, L.; Cameron, C. G.; Mcfarland, S. A. *Chem. Rev.* **2019**, *119*, 797–828.

[13] Https://clinicaltrials.gov/ct2/show/NCT03945162?term=TLD-1433&rank=1. (accessed the 27/ 09/ 2019).

[14] Griffith, C. A.; Dayoub, A.; Janaratne, T.; Alatrash, N.; Abayan, K.; Mohamedi, A.; Breitbach, Z.; Armstrong, D. W.; MacDonnell, F. M. *Chem. Sci.* **2017**, *8*, 3726–3740.

[15] Poynton, F. E.; Bright, S. A.; Blasco, S.; Williams, D. C.; Kelly, J. M.;

Gunnlaugsson, T. *Chem Soc Rev* **2017**, *46*, 7706–7756.

[16] Notaro, A.; Gasser, G. *Chem. Soc. Rev.* **2017**, *46*, 7317–7337.

[17] Notaro, A.; Frei, A.; Rubbiani, R.; Jakubaszek, M.; Basu, U.; Koch, S.; Mari, C.; Dotou, M.; Blacque, O.; Gouyon, J.; et al. *ChemRxiv. Prepr.* **2019**.

[18] CHEW, L. F. B. and H. *Mutat. Res.* **1979**, *67*, 367–371.

[19] Ito, H. *Agric. Biol. Chem.* **1977**, *41*, 1307–1308.

[20] I--food, C.; Services, H. *CFR Code Fed. Regul.* **2018**, *3*, 1–18.

[21] Bingham, A. F.; Birch, G. G.; Graaf, C. De; Behan, J. M.; Perring, K. D. *Chem. Senses* **1990**, *15*, 447–456.

[22] Kahn, V.; Schved, F.; Lindner, P. *J. Food Biochem.* **1993**, *17*, 217–233.

[23] Nelson, W. O.; Karpishin, T. B.; Rettig, S. J.; Orvig, C. *Inorg. Chem.* **1988**, *27*, 1045–1051.

[24] Lucio, P. C.; Nicholas, G.; Geoffrey, G. F.; Huali, H.; Mcneill, J. H.; Rettig, S. J.; Setyawati, I. A.; Shuter, E.; Sun, Y.; Tracey, A. S.; et al. *J. Am. Chem. Soc.* **1995**, *117*, 12759–12770.

[25] Ellis, B. L.; Duhme, A. K.; Hider, R. C.; Hossain, M. B.; Rizvi, S. *J. Med. Chem.* **1996**, *2623*, 3659–3670.

[26] Lord, S. J.; Epstein, N. A.; Paddock, R. L.; Vogels, C. M.; Hennigar, T. L.; Zaworotko, M. J.; Taylor, N. J.; Driedzic, W. R.; Broderick, T. L.; Westcott, S. A. *Can. J. Chem.* **1999**, *1261*, 1249–1261.

[27] Thompson, K. H.; Barta, C. A.; Orvig, C.; Thompson, K. *Chem. Soc. Rev* **2006**, *35*, 545–556.

[28] Thompson, K. H.; Chiles, J.; Yuen, V. G.; Tse, J.; Mcneill, J. H.; Orvig, C. *J. Inorg. Biochem.* **2004**, *98*, 683–690.

[29] Dömötör, O.; Aicher, S.; Schmidlehner, M.; Novak, M. S.; Roller, A.; Jakupec, M. A.; Kandioller, W.; Hartinger, C. G.; Keppler, B. K.; Enyedy, É. A. *J. Inorg. Biochem.* **2014**, *134*, 57–65.

[30] Kandioller, W.; Hartinger, C. G.; Nazarov, A. A.; Bartel, C.; Skocic, M.; Jakupec, M. A.; Arion, V. B.; Keppler, B. K. *Chem. Eur. J* **2009**, 12283–12291.

[31] Fang, L.; Ming, S.; Ling, H.; Soo, K.; Vikneswaran, R.; Guan, S.; Ahmad, M.; Alan, S.; Jamil, M.; Hee, C. *J. Inorg. Biochem.* **2011**, *105*, 339–347.

[32] Reddy, V. D.; Dayal, D.; Szalda, D. J.; Cosenza, S. C.; Reddy, M. V. R. *J. Organomet. Chem.* **2012**, *700*, 180–187.

[33] Murakami, K.; Ishida, K.; Watakabe, K.; Tsubouchi, R.; Naruse, M.; Yoshino, M. *Toxicol. Lett.* **2006**, *161*, 102–107.

[34] Hironishi, M.; Kordek, R.; Yanagihara, R.; Garruto, R. M. *Neurodegeneration* **1996**, *5*, 325–329.

[35] Yasumoto, E.; Nakano, K.; Nakayachi, T.; Morshed, S. R.; Hashimoto, K. E. N.; Kikuchi, H.; Nishikawa, H.; Kawase, M.; Sakagami, H. *Anticancer Res.* **2004**, *762*, 755–762.

[36] Barrand, M. A.; Callingham, B. A. *Br. J. Pharmacol.* **1991**, *102*, 408–414.

[37] Barrand, M. A.; Hider, R. C.; Callingham, B. A. *J. Pharm. Pharmacol.* **1990**, *42*, 105–107.

[38] Thompson, K. H.; Lichter, J.; Lebel, C.; Scaife, M. C.; Mcneill, J. H.; Orvig, C. *J. Inorg. Biochem.* **2009**, *103*, 554–558.

[39] Thompson, K. H.; Liboiron, Æ. B. D.; Sun, Æ. Y.; Patrick, B. O.; Karunaratne, Æ. V.; Rawji, Æ. G.; Cassidy, C.; Mcneill, Æ. J. H.; Yuen, Æ. V. G. *J. Biol. Inorg. Chem.* **2003**, *8*, 66–74.

[40] Thompson, K. H.; Orvig, C. *J. Chem. Soc., Dalt. Trans.* **2000**, 2885–2892.

[41] Crans, D. C.; Schoeberl, S.; Roess, D. A. *J. Biol. Inorg. Chem.* **2011**, *16*, 961–972.

[42] Bernstein, L. R.; Tanner, T.; Godfrey, C.; Noll, B.; Road, W.; Park, M. *Met. Based. Drugs* **2000**, *7*, 33–47.

[43] Jakupec, M. A.; Keppler, B. K. *Curr. Top. Med. Chem.* **2004**, *4*, 1575–1583.

[44] Chitambar, C. R.; Purpi, D. P.; Woodliff, J.; Yang, M.; Wereley, J. P. *J. Pharmacol. Exp. Ther.* **2007**, *322*, 1228–1236.

[45] Enyedy, É. A.; Dömötör, O.; Bali, K.; Keppler, B. K. *J. Biol. Inorg. Chem.* **2015**, *20*, 77–88.

[46] Deleon, K.; Balldin, F.; Watters, C.; Hamood, A.; Griswold, J.; Sreedharan, S.; Rumbaugh, K. P. *Antimicrob. Agents Chemother.* **2009**, *53*, 1331–1337.

[47] Id, L. G.; Id, L. R. B.; Haynes, A. M.; Godornes, C.; Ciccarese, G.; Drago, F.; Parodi, A.; Valdevit, S.; Anselmi, L.; Tomasini, C. F.; et al. *PLoS Negl. Trop. Dis.* **2019**, 1–14.

[48] Chitambar, C. R.; Al-gizawiy, M. M.; Alhajala, H. S.; Pechman, K. R.; Wereley, J. P.; Wujek, R.; Clark, P. A.; Kuo, J. S.; Antholine, W. E.; Schmainda, K. M. *Mol. Cancer Ther.* **2018**, No. 12, 1–12.

[49] Chua, M.; Bernstein, L. R.; Li, R. U. I.; So, S. K. S. *Anticancer Res.* **2006**, *1744*, 1739–1743.

[50] Kandioller, W.; Hartinger, C. G.; Nazarov, A. A.; Kasser, J.; John, R.; Jakupec, M. A.; Arion, V. B.; Dyson, P. J.; Keppler, B. K. *J. Organomet. Chem.* **2009**, *694*, 922–929.

[51] Hartinger, C. G.; Eichinger, R. E.; Stolyarova, N.; Severin, K.; Jakupec, M. A.; Nazarov, A. A.; Keppler, B. K. *Organometallics* **2008**, *27*, 2405–2407.

[52] Brastos, I.; Alessio, E.; Ringenberg, M. E.; Rauchfuss, T. B. *Inorg. Synth.* **2010**, *35*, 148–163.

[53] Caspar, R.; Cordier, C.; Waern, J. B.; Guyard-Duhayon, C.; Gruselle, M.; Le Floch, P.; Amouri, H. *Inorg. Chem.* **2006**, *45*, 4071–4078.

[54] Haga, M.; Dodsworth, E. S.; Lever, A. B. P. *Inorg. Chem.* **1986**, *25*, 447–453.

[55] Higgins, S. L. H.; White, T. A.; Winkel, B. S. J.; Brewer, K. J. *Inorg. Chem.* **2011**, *50*, 463–470.

[56] Sobota, P.; Przybylak, K.; Utko, J.; Jerzykiewicz, L. B.; Pombeiro, A. J. L.; Guedes Da Silva, M. F. C.; Szczegot, K. *Chem. Eur. J.* **2001**, *7*, 951–958.

[57] Patra, M.; Joshi, T.; Pierroz, V.; Ingram, K.; Kaiser, M. *Chem. Eur. J.* **2013**, *19*, 14768–14772.

[58] Hall, M. D.; Telma, K. A.; Chang, K.-E.; Lee, T. D.; Madigan, J. P.; Lloyd, J. R.; Goldlust, I. S.; Hoeschele, James D. Gottesman, M. M. *Cancer Res.* **2014**, *74*, 3913–3922.

[59] Huang, H.; Humbert, N.; Bizet, V.; Patra, M.; Chao, H. *J. Organomet. Chem.* **2017**, *839*, 15–18.

[60] Lakowicz, J. R. *Principles of Fluorescence Spectroscopy*; 2006.

[61] Pierroz, V.; Joshi, T.; Leonidova, A.; Mari, C.; Schur, J.; Ott, I.; Spiccia, L.; Ferrari, S.; Gasser, G. *J. Am. Chem. Soc.* **2012**, *134*, 20376–20387.

[62] Bruce, S. J.; Tavazzi, I.; Rezzi, S.; Kochhar, S.; Guy, P. A. **2009**, *81*, 3285–3296.

[63] Frei, A.; Rubbiani, R.; Tubafard, S.; Blacque, O.; Anstaett, P.; Felgenträger, A.; Maisch, T.; Spiccia, L.; Gasser, G. *J. Med. Chem.* **2014**, *57*, 7280–7292.

[64] Cepeda, V.; Fuertes, M.; Castilla, J.; Alonso, C.; Quevedo, C.; Perez, J. *Anticancer. Agents Med. Chem.* **2007**, *7*, 3–18.

[65] Keizer, H. G.; Pinedo, H. M.; Schuurhuis, G. J.; Joenje, H. *Pharmac. Ther* **1990**, *47*, 219–231.

[66] Kelm, J. M.; Timmins, N. E.; Brown, C. J.; Fussenegger, M.; Nielsen, L. K. *Biotechnol. Bioeng.* **2003**, *83*, 173–180.

[67] Ma, H.; Jiang, Q.; Han, S.; Wu, Y.; Tomshine, J. C.; Wang, D.; Gan, Y.; Zou, G. *Mol. Imaging* **2012**, *11*, 487–498.

[68] Kapałczyńska, M.; Kolenda, T.; Przybyła, Weronika Zajączkowska, Maria Teresiak, A.; Filas, V.; Ibbs, M.; Bliźniak, R.; Łuczewski, Łukasz Lamperska, K. *Arch. Med. Sci.* **2018**, *4*, 910–919.

[69] Friedrich, J.; Seidel, C.; Ebner, R.; Kunz-schughart, L. A. *Nat. Protoc.* **2009**, *4*, 309–324.

[70] Hess, J.; Huang, H.; Kaiser, A.; Pierroz, V.; Blacque, O. **2017**, No. Ii, 9888–

9896.

[71] Seo, O. W.; Kim, M.; Hulme, J.; An, S. S. A. **2016**, 7207–7218.

[72] Belmokhtar, A. C.; Hillion, J.; Ségal-Bendirdjian, E. *Oncogene* **2001**, 3354–3362.

[73] Zeng, L.; Chen, Y.; Huang, H.; Wang, J.; Zhao, D.; Ji, L.; Chao, H. *Chemistry* **2015**, *21*, 15308–15319.

[74] Zisowsky, J.; Koegel, S.; Leyers, S.; Devarakonda, K.; Kassack, M. U.; Osmak, M.; Jaehde, U. *Biochem. Pharmacol.* **2007**, *73*, 298–307.

[75] Dedov, V. N.; Cox, G. C.; Roufogalis, B. D. *Micron* **2001**, *32*, 653–660.

[76] Zorova, L. D.; Popkov, V. A.; Plotnikov, E. Y.; Silachev, D. N.; Pevzner, B.; Jankauskas, S. S.; Babenko, V. A.; Zorov, S. D.; Balakireva, A. V; Juhaszova, M.; et al. *Anal. Biochem.* **2018**, No. 552, 50–59.

[77] Sakamuru, S.; Attene-ramos, M. S.; Xia, M. Mitochondrial Membrane Potential Assay. In *High-Throughput Screening Assays in Toxicology, Methods in Molecular Biology,*; 2016; Vol. 1473, pp 17–22.

[78] Terada, H. *Environ. Health Perspect.* **1990**, *87*, 213–218.

[79] Fulmer, G. R.; Miller, A. J. M.; Sherden, N. H.; Gottlieb, H. E.; Nudelman, A.; Stoltz, B. M.; Bercaw, J. E.; Goldberg, K. I. *Organometallics* **2010**, *29*, 2176–2179.

[80] Krachler, M. *J. Environ. Monit.* **2007**, *9*, 790–804.

[81] Mari, C.; Pierroz, V.; Rubbiani, R.; Patra, M.; Hess, J.; Spingler, B.; Oehninger, L.; Schur, J.; Ott, I.; Salassa, L.; et al. *Chem. Eur. J.* **2014**, *20*, 1–17.

[82] Beaven, G. H.; Chen, S.; Albis, A. D.; Gratzer, W. B. *Eur. J. Biochem.* **1974**, *546*, 539–546.

[83] Gans, P.; Sabatini, A.; Vacca, A. *Talanta Investig.* **1996**, *43*, 1739–1753.

[84] Domotor, O.; Hartinger, C. G.; Bytzek, A. K.; Kiss, T.; Keppler, B. K.; Enyedy, E. A. *J. Biol. Inorg. Chem.* **2013**, *18*, 9–17.

[85] Https://rockland-inc.com/Nuclear-Extract-Protocol.aspx. (accessed the 03.10.2019).

[86] Tharaud, M.; Gardoll, S.; Khelifi, O.; Benedetti, M. F.; Sivry, Y. *Microchem. J.* **2015**, *121*, 32–40.

Supplementary Information

A maltol-containing Ruthenium Polypyridyl Complex as a Potential Anticancer Agent

Anna Notaro,[a] Marta Jakubaszek,[a, b] Severin Koch,[c] Riccardo Rubbiani,[c] Orsolya Dömötör,[d] Éva A. Enyedy,[d, e] Mazzarine Dotou,[a] Fethi Bedioui,[f] Mickaël Tharaud,[g] Bruno Goud,[b] Stefano Ferrari,[h,i] Enzo Alessio,[j] and Gilles Gasser*[a]

[a] *Chimie ParisTech, PSL University, CNRS, Institute of Chemistry for Life and Health Sciences, Laboratory for Inorganic Chemical Biology, F-75005 Paris, France.*

[b] *Institut Curie, PSL University, CNRS UMR 144, Paris, France.*

[c] *Department of Chemistry, University of Zurich, Winterthurerstrasse 190, 8057 Zurich, Switzerland.*

[d] *Department of Inorganic and Analytical Chemistry, Interdisciplinary Excellence Centre, University of Szeged, Dóm tér 7. H-6720 Szeged, Hungary.*

[e] *MTA-SZTE Momentum Functional Metal Complexes Research Group, University of Szeged, Dóm tér 7, H-6720 Szeged, Hungary.*

[f] *Chimie ParisTech, PSL University, CNRS, Institute of Chemistry for Life and Health Sciences, Team Synthèse, Electrochimie, Imagerie et Systèmes Analytiques pour le Diagnostic, F-75005 Paris, France.*

[g] *Université de Paris, Institut de physique du globe de Paris, CNRS, F-75005 Paris, France.*

[h] *Institute of Molecular Cancer Research, University of Zurich, Zurich, Switzerland.*

[i] *Institute of Molecular Genetics of the Czech Academy of Sciences, Videnska 1083, 143 00 Prague, Czech Republic.*

[j] *Department of Chemical and Pharmaceutical Sciences, University of Trieste, Via L. Giorgieri 1, 34127 Trieste, Italy.*

* Corresponding author: E-mail: gilles.gasser@chimeparistech.psl.eu; WWW: www.gassergroup.com; Phone: +33 1 44 27 56 02

Table of Contents

1) Figure S1. NMR spectra of **[Ru(DIP)$_2$(mal)](PF$_6$)**

[Ru(DIP)$_2$(mal)](PF$_6$), ^{1}H, CD_2Cl_2, 400 MHz

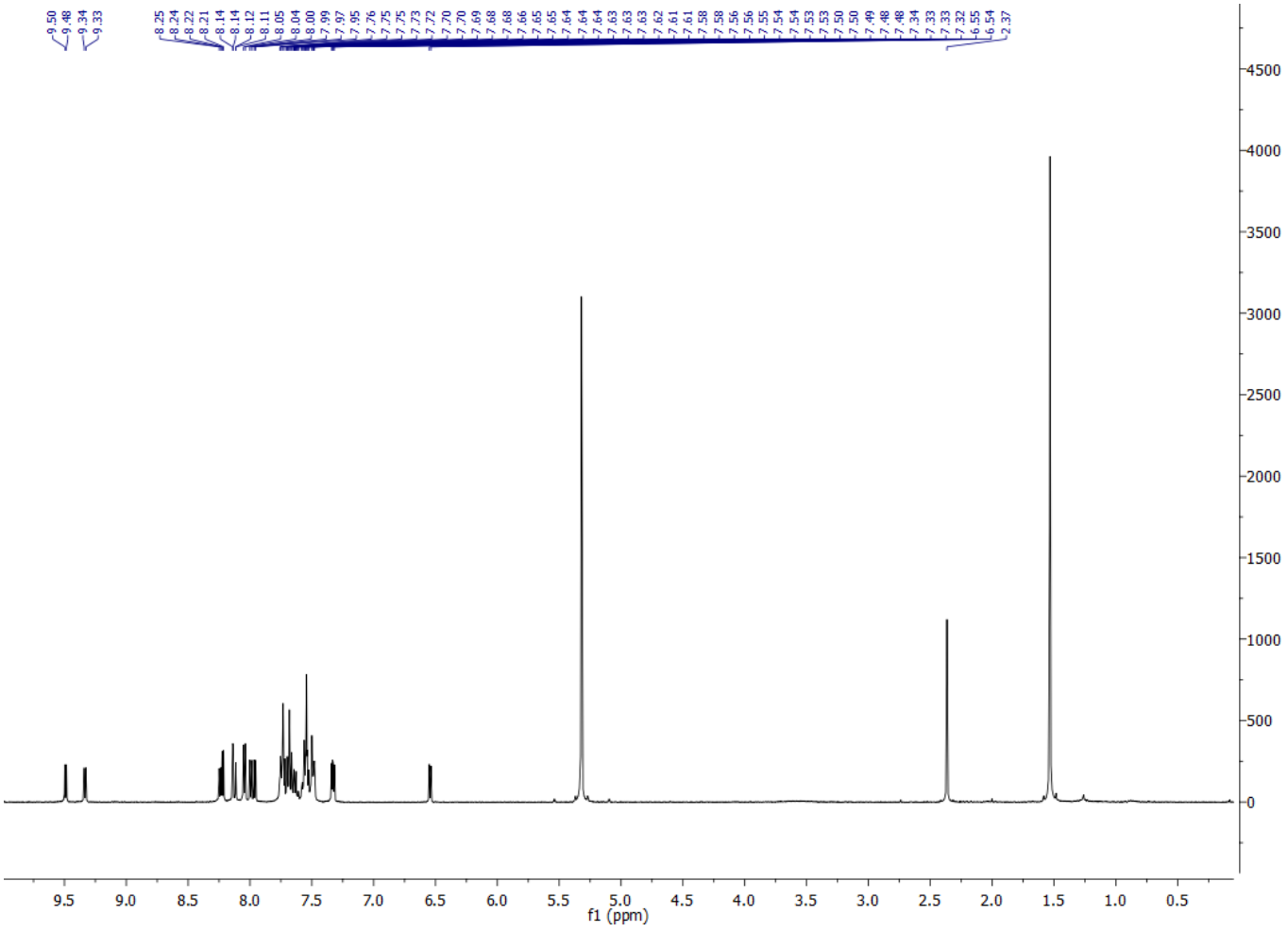

[Ru(DIP)$_2$(mal)](PF$_6$), $^{13}C\{^1H\}$, CD_2Cl_2, 125 MHz

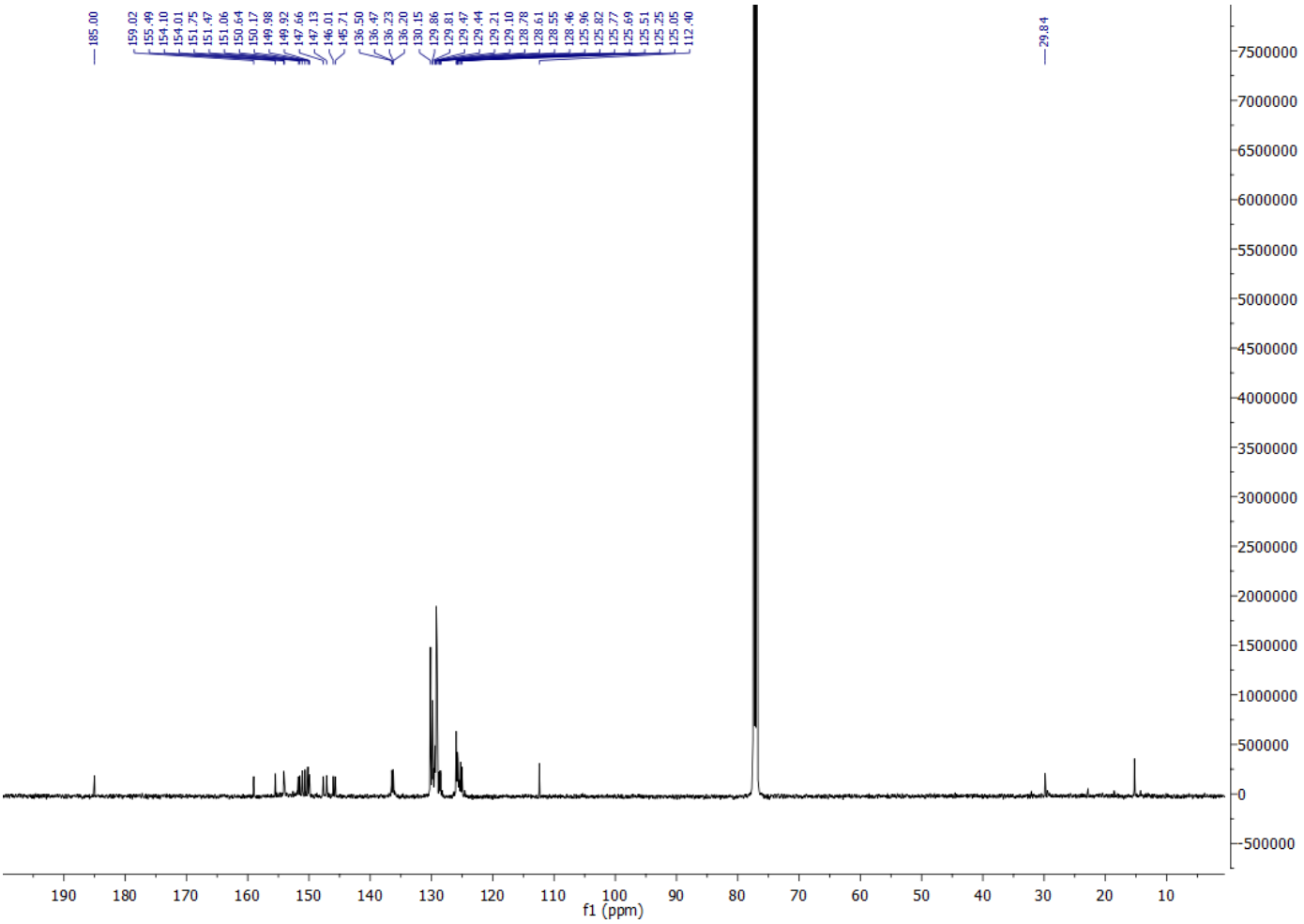

2) Figure S2. Voltammograms recorded by CV (upper figure) and with the use of RDE (lower figure) for **[Ru(DIP)$_2$(mal)](PF$_6$)** (from -2.1 to +1 V) with a glassy carbon electrode in DMF (1 mM) containing Bu_4NPF_6 (100 mM) as supporting electrolyte and decamethylferrocene as an internal standard (0.25 mM). Data were recorded versus saturated calomel electrode at scan rate of 100 mV/s and recalculated versus $Me_{10}Fc^{0/+}$ potential value (feature marked with * in Figure S2).

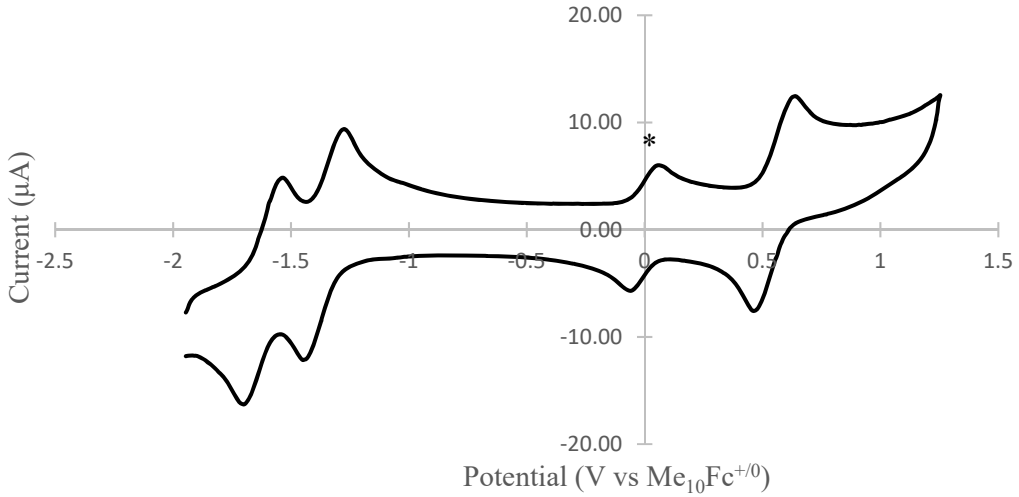

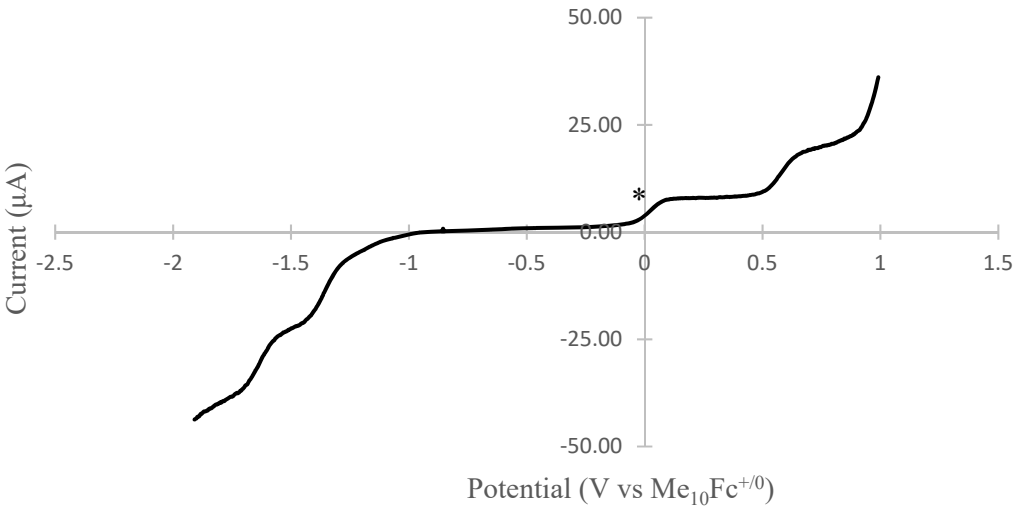

3) Table S1. Electrochemical data for **$[Ru(DIP)_2(mal)](PF_6)$**.

		$DIP^{0/-}$	**$DIP^{0/-}$**	**$Ru^{III/II}$**
$[Ru(DIP)_2(mal)](PF_6)$	**$E_{1/2}$[a] [V] (RDE)**	-1.636 ±0.020	-1.341 ± 0.017	+0.566 ± 0.037
	$E_{1/2}$[b] [V] (CV)	-1.624 ± 0.030	-1.358 ± 0.004	+0.550 ± 0.005

[a] $E_{1/2}$ = half-wave.
[b] $E_{1/2} = (E_{Pa} + E_{Pc})/2$.

4) Figure S3. Overlap of the ^{1}H spectra (downfield region) of **[Ru(DIP)$_2$(mal)](PF$_6$)** in DMSO-d$_6$ at room temperature over 42h.

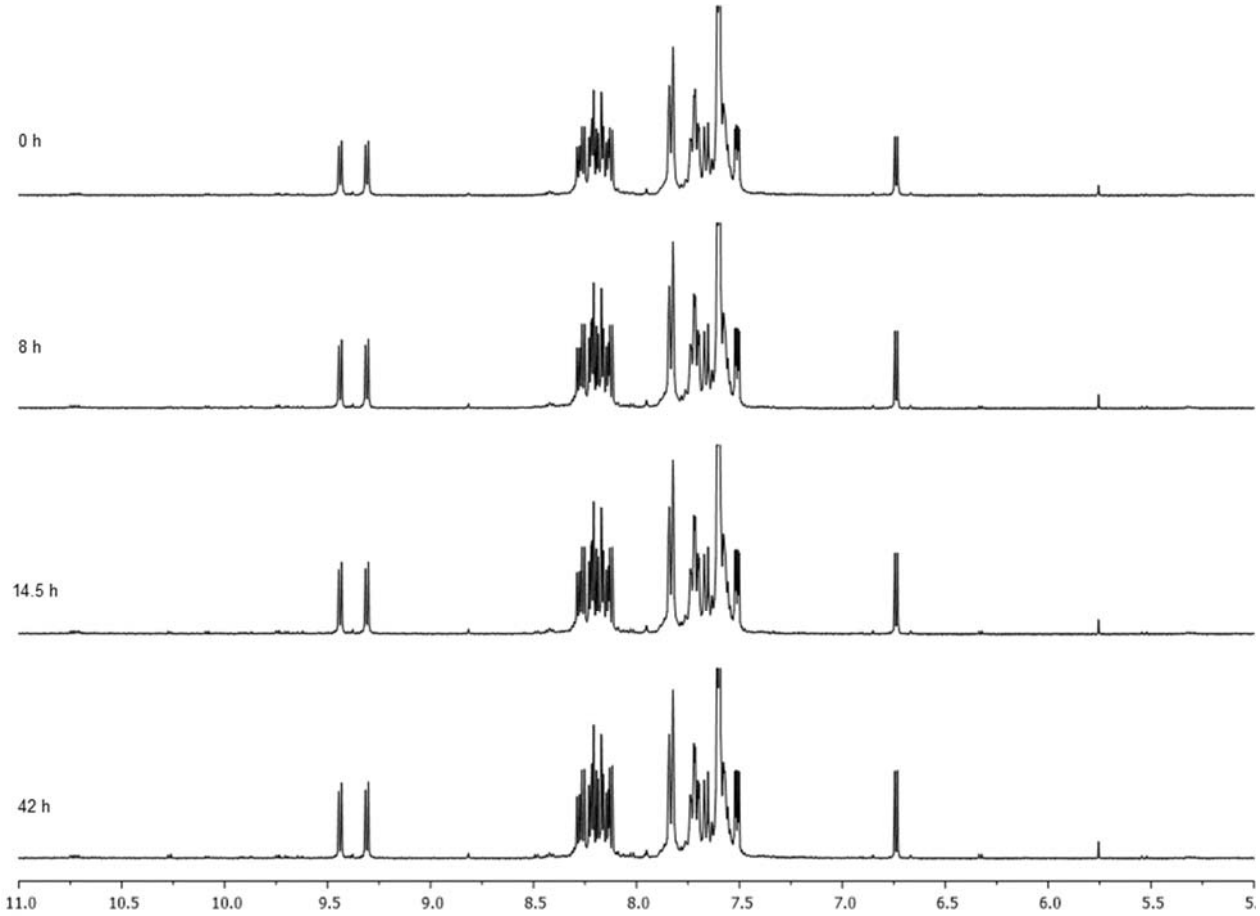

5) Detailed investigation on the stability of the complex in different solvents and conditions.

Poor water solubility of **[Ru(DIP)$_2$(mal)](PF$_6$)** prevented direct preparation of aqueous samples. Low molecular mass components of the blood serum are often able to solubilize metal complexes as a result of ligand exchange interactions. RPMI 1640 cell culture medium, containing phosphate and hydrogen carbonate buffered saline, inorganic ions Ca^{2+}, Mg^{2+}, K^+, Na^+, glucose, essential and some non-essential amino acids in higher concentration, was also not suitable to dissolve **[Ru(DIP)$_2$(mal)](PF$_6$)** in aqueous medium. Therefore, stock solutions prepared in ethanol or in methanol were used for further sample preparation; final samples contained ≤ 2% (v/v) alcohol. The alcoholic (ethanol or methanol) stock solutions showed only slight spectral changes within 6 h (Fig. S4/B). The sample in pure ethanol was well filterable by ultrafilter devices and ~100% of the complex could be found in the filtered (bottom) fraction. By ultrafiltration of aqueous samples (containing ~ 2% (v/v) ethanol), complex stuck to the filter membrane, that allowed us to study the possible appearance of liberated maltol ligand in the filtrate fraction (maltol itself is well filterable). Filtrate fraction of samples filtered immediately after preparation and after 6 h waiting, showed low absorbances (see Fig. S4/C/inset for HEPES buffered sample after 6 h) in the studied wavelength range suggesting that the complex stuck to the filter and did not decompose (i.e. no ligand dissociation occurred).

Spectral changes observed in HEPES and phosphate buffers refer to only moderate changes in the complex structure. Aggregation followed by precipitation of the complex is a possible explanation for that. As next step the effect of oxidative, oxygen-free or reductive conditions were investigated; oxygen or argon was bubbled through HEPES buffered samples or 50 eq (1 mM) of GSH was added to the sample containing the **[Ru(DIP)$_2$(mal)](PF$_6$)** complex. In Fig. S5/A and B oxygenated sample shows faster and more pronounced spectral changes compared to the only HEPES buffered sample. Data are shown for samples containing no precipitation. In the oxygenated sample precipitation occurred after 1 h. On the other hand, applying argon atmosphere or the addition of biological reductant GSH seem to prevent partially the spectral changes and delay the concomitant precipitation of the complex (Fig. S5). ^{1}H NMR spectra recorded for samples containing 1 mM **[Ru(DIP)$_2$(mal)](PF$_6$)** complex in methanol-d_4 or in phosphate buffer – methanol-d_4 70:30 (V/V) solvent mixture did not show the appearance of free, non-coordinated maltol or 4,7-diphenyl-1,10-phenantroline, however precipitation occurred in the buffered sample under these conditions providing no reliable result on the solution chemistry of this compound.

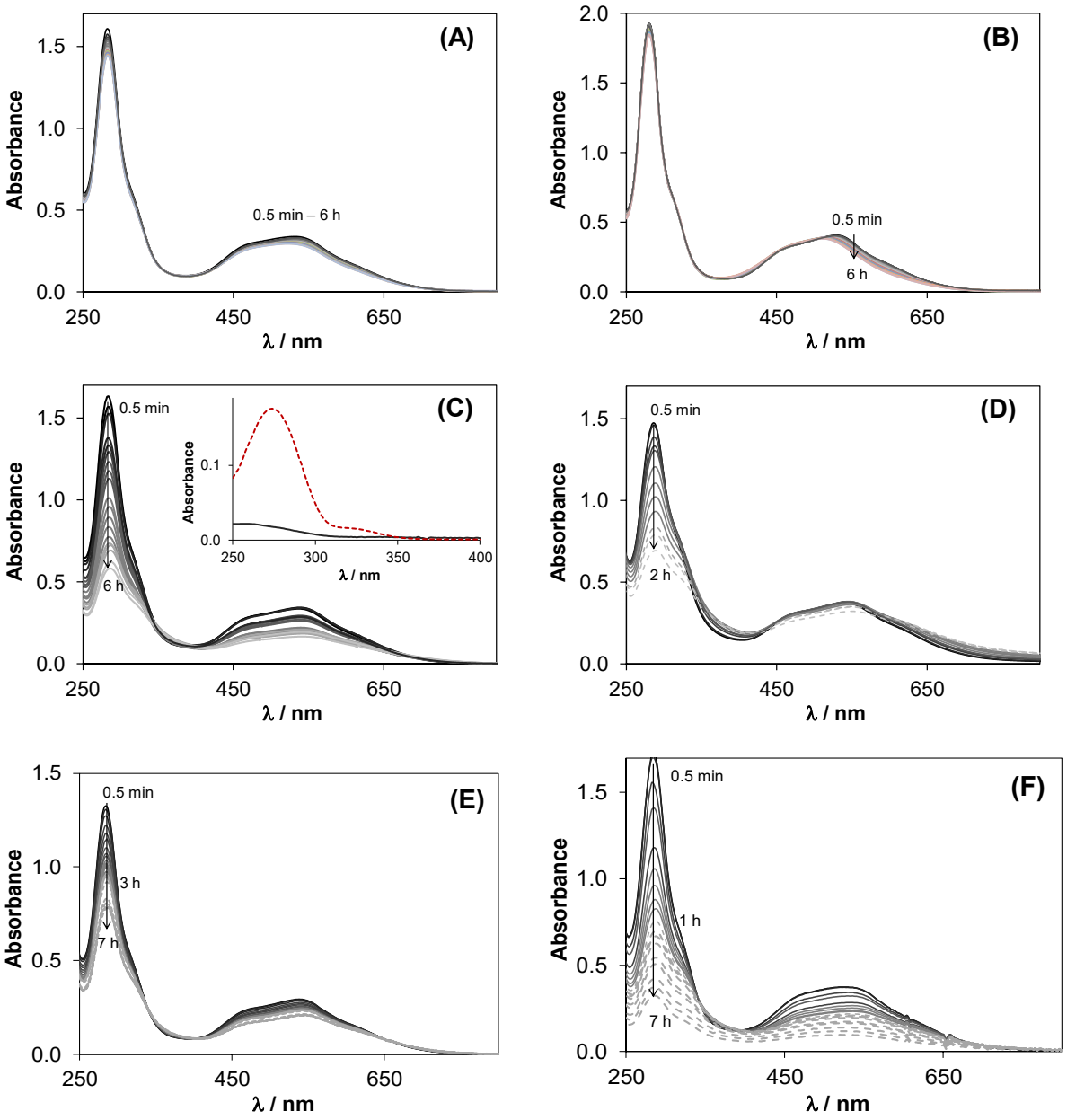

Figure S4. Time-dependent UV-Vis absorbance spectra of $[Ru(DIP)_2(mal)](PF_6)$ followed in water/ethanol (pH ~ 8) (A); ethanol (B); 20 mM HEPES/ethanol (pH = 7.4) (C); 20 mM phosphate/ethanol (pH = 7.40) (D); and under argon atmosphere (E) or in oxygen atmosphere (F) in 20 mM HEPES/ethanol (pH = 7.40). Grey dashed spectra refer to the appearance of precipitation. Inset in (C) shows the spectrum of filtrate fraction of sample (C) after 6 h (solid black line) and calculated spectrum (dashed red line) of maltol which should be detected at 100% decomposition of the original complex (19.8 µM maltol) {c_{compex} = 19.8 µM (A,C,D) or 21.7 µM (B,F) or 17.2 µM (E), 2% ethanol (v/v) (in A,C-F), pure ethanol (B); T = 25 °C}.

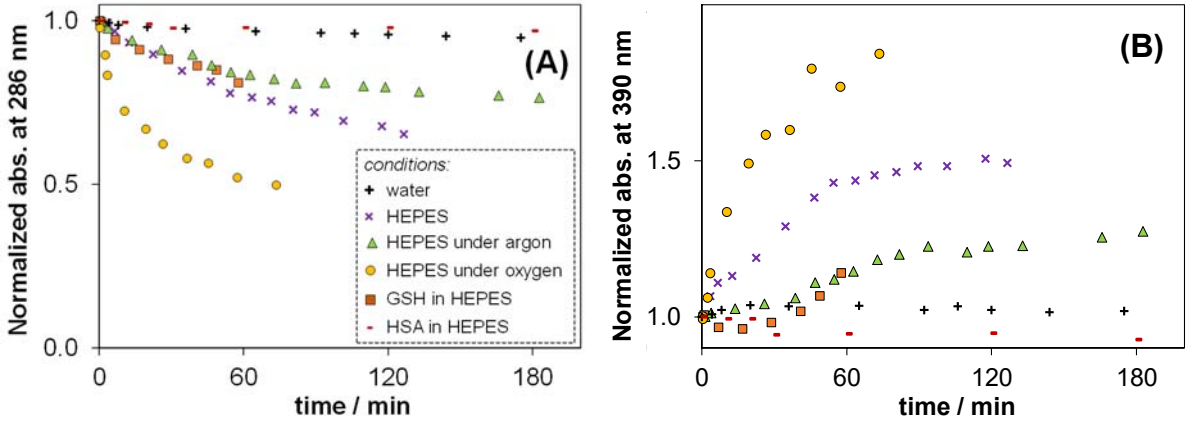

Figure S5. Normalized absorbance values as a function of time at 286 nm (A) and 390 nm (B) at the indicated conditions. Data are shown until no precipitation occurred in the samples. {$c_{compex} \approx 20$ µM, $c_{HSA} = 100$ µM, $c_{GSH} = 1$ mM, 2% ethanol (v/v), T = 25 °C}

6) **More details on interaction with human serum albumin**

The presence of human serum albumin (HSA) hindered the precipitation of **[Ru(DIP)$_2$(mal)](PF$_6$)** in 20 mM phosphate and HEPES buffered samples, and no liberation of maltol or 4,7-diphenyl-1,10-phenantroline was detected in ultrafiltration experiments.

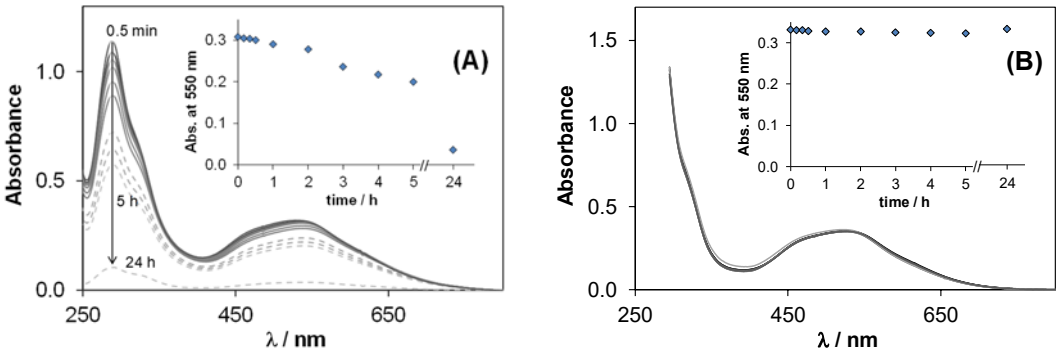

Figure S6. UV-Vis absorbance spectra of **[Ru(DIP)$_2$(mal)](PF$_6$)** followed in RPMI 1640 cell culture medium (A) and in 20 mM phosphate buffer containing 100 μM HSA (B). Insets show the time course of the absorbance changes at 550 nm. Dashed spectra refer to precipitation of the complex. {c_{compex} = 13.8 μM; 2% ethanol (V/V); pH = 7.40; T = 25 °C}.

Binding via intermolecular binding is supported by the UV-Vis spectra of **[Ru(DIP)$_2$(mal)](PF$_6$)** recorded in the presence of increasing amount of HSA (see Fig. S8), where practically no spectral changes can be observed, except upon the addition of the first 0.03 eq of HSA. Notably, binding of a small molecule on HSA via secondary binding interactions often does not result in any alteration of UV-Vis absorbance bands.

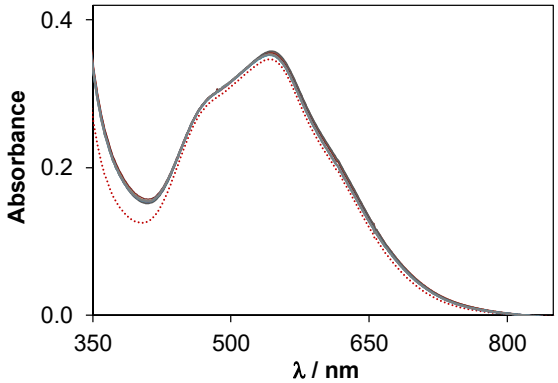

Figure S7. UV-Vis absorbance spectra of **[Ru(DIP)$_2$(mal)](PF$_6$)** alone (red dotted spectrum) and in the presence of 0.03-2.0 eq of HSA (grey scale spectra). Spectra are subtracted by the spectrum of HSA. {c_{compex} = 20.0 μM; 2% ethanol (V/V); pH = 7.40 (20 mM phosphate buffer); T = 25 °C}

Binding at sites I and II was investigated by spectrofluorimetry via Trp214 quenching and via dansylglycine (DG) displacement experiments, respectively. Following the selective excitation of Trp214 at 295 nm, its

fluorescence emission intensity can be attenuated by the binding of a guest molecule at site I. Intermolecular binding processes usually take place very fast (within seconds), and indeed our time dependent measurement indicated fast kinetics at this site; therefore spectra were recorded after 5 min waiting time. Emission spectra in Fig. S9 show a definite increase of fluorescence, instead of quenching, upon addition of **[Ru(DIP)$_2$(mal)](PF$_6$)** to HSA. The increase can be explained by the complete overlapping of the low intrinsic fluorescence of the metal complex with the protein Trp emission band.

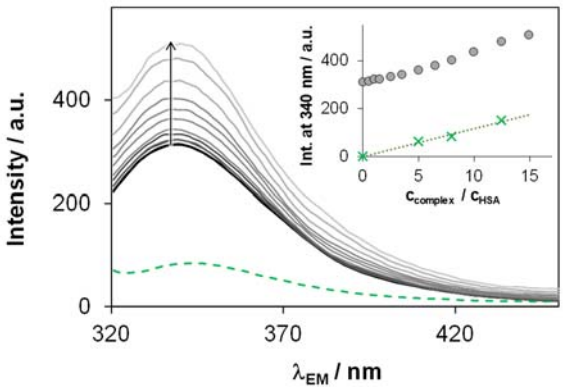

Figure S8. Changes of Trp214 fluorescence in HSA in the presence of **[Ru(DIP)$_2$(mal)](PF$_6$)**, green dashed spectrum denotes the emission of 8 μM metal complex alone. Inset shows the relative emission intensities at 340 nm for HSA– **[Ru(DIP)$_2$(mal)](PF$_6$)** system (●) and for **[Ru(DIP)$_2$(mal)](PF$_6$)** alone (×). {c_{HSA} = 1 μM; $c_{complex}$ = 0–15 μM; pH = 7.40 (20 mM phosphate buffer); < 2% ethanol λ_{EX} = 295 nm; T = 25 ◦C}.

The HSA−DG adduct emits light intensively and displacement of DG by other small molecules results in a considerable decrease in the emission intensity, as it is detailed in the main text DG is gradually displaced by **[Ru(DIP)$_2$(mal)](PF$_6$)** at site II.

Experimental for the ultrafiltration and circular dichroism studies

Ultrafiltration studies were carried out in Amicon Ultra-0.5 (Millipore cutoff: 10 kDa) filter devices. 0.5 or 1.0 mL portions were filtered with an Eppendorf MiniSpin plus centrifuge (relative centrifugal force ~8000 g; 5–10 min) and the UV–vis spectrum of the filtrate (bottom fraction) was compared to the reference spectra of the original sample or to the ligand spectra. Circular dichroism (CD) spectra for the metal complex – HSA systems were recorded on a Jasco J-815 spectrometer in the wavelength interval from 250 to 1000 nm. Samples contained 24 μM metal complex at pH 7.40 (20 mM HEPES buffer) and increasing amount of HSA (0 – 50 μM) using quartz cell of 1 cm path length.

7) Figure S9. a) RP-UPLC traces of **[Ru(DIP)$_2$(mal)](PF$_6$)** (0.12 mM) incubated in human plasma at 37 °C, using caffeine (1.92 mM) as internal standard, recorded at 275 nm. b) Percentage concentration of **[Ru(DIP)$_2$(mal)](PF$_6$)**, normalized with respect to the internal standard and plotted against time.

a)

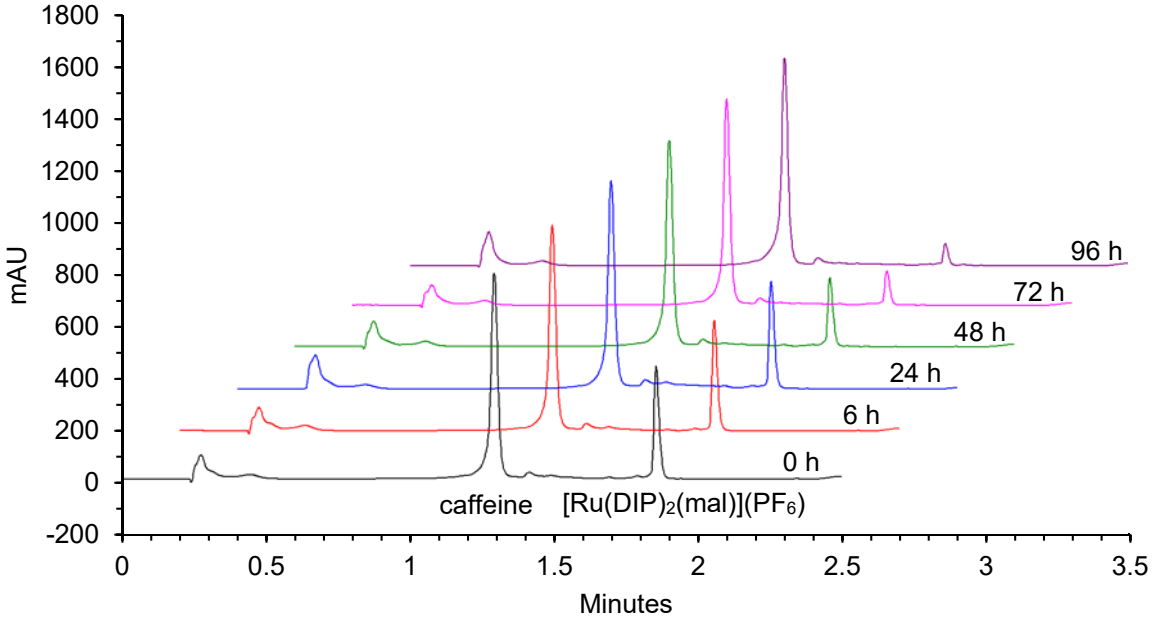

b)

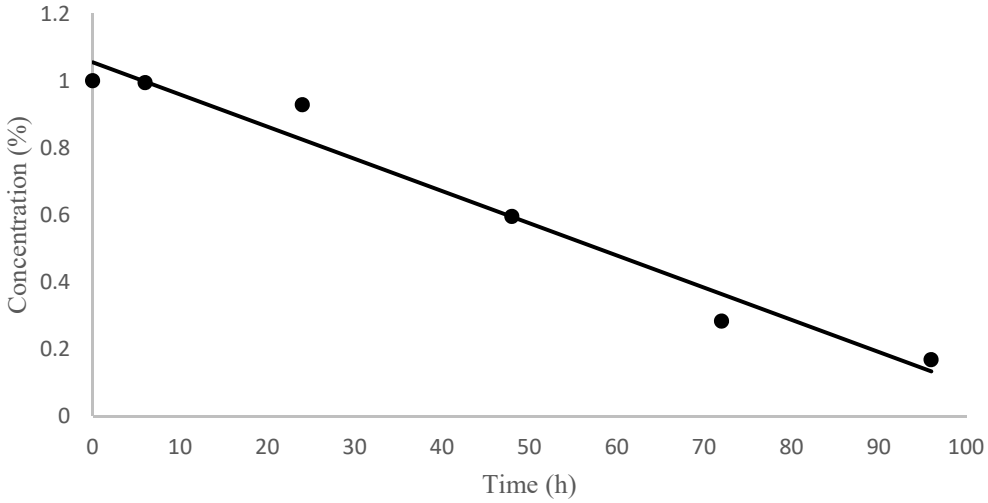

8) Figure S10. Evaluation of the cytotoxicity in 2D cell culture models *via* fluorometric cell viability assay.

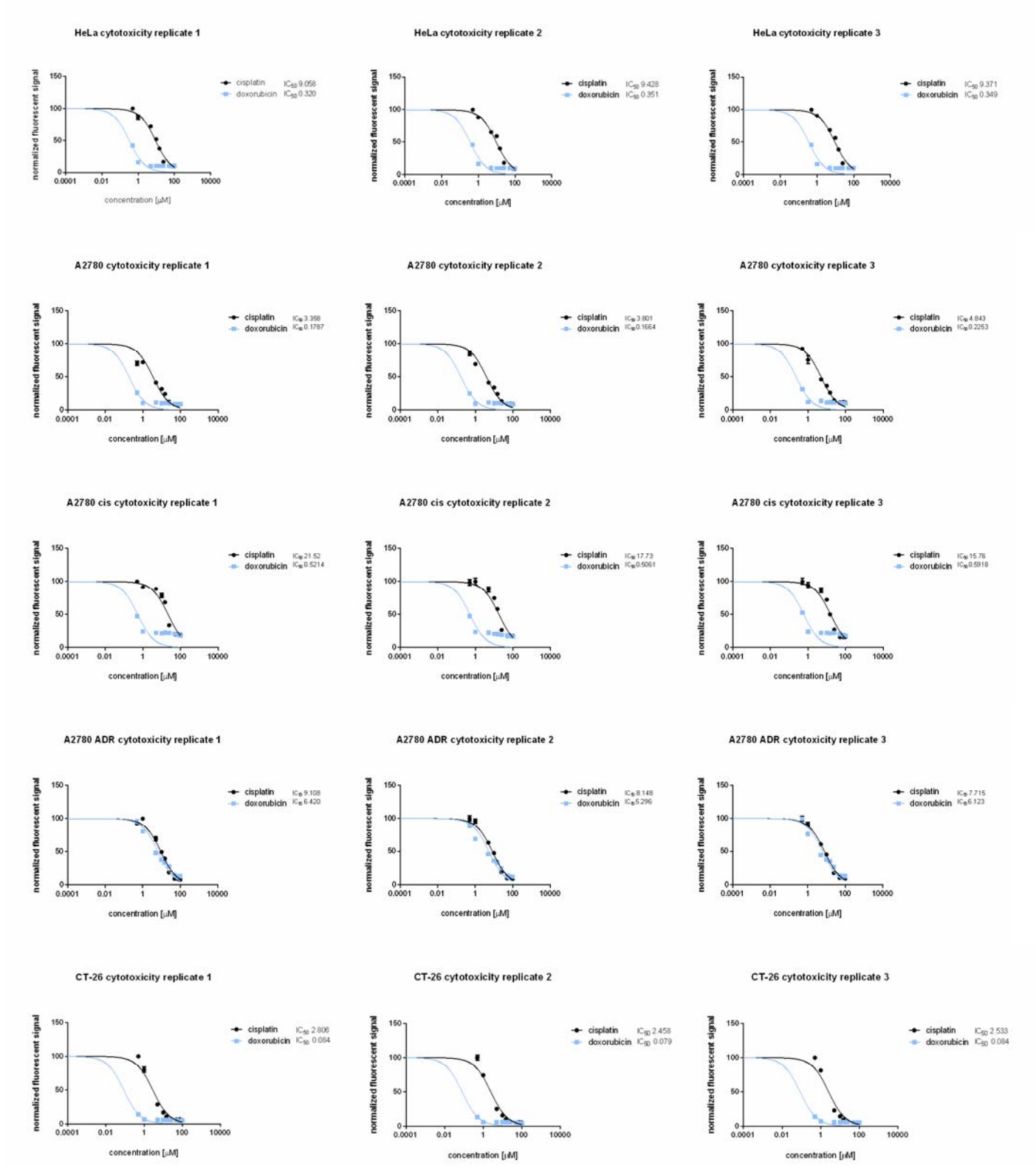

CT-26 LUC cytotoxicity replicate 1

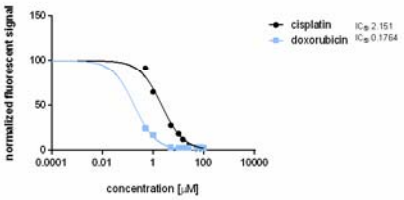

CT-26 LUC cytotoxicity replicate 2

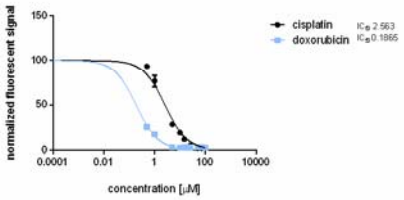

CT-26 LUC cytotoxicity replicate 3

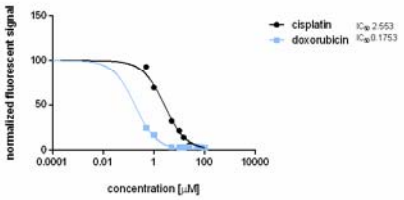

RPE-1 cytotoxicity replicate 1

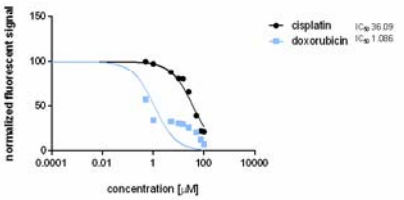

RPE-1 cytotoxicity replicate 2

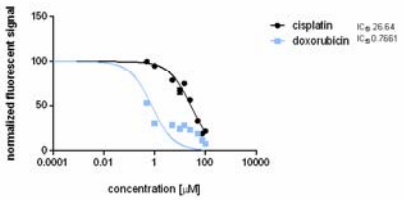

RPE-1 cytotoxicity replicate 3

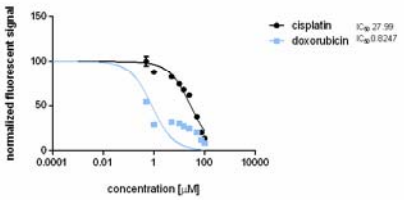

HeLa cytotoxicity replicate 1

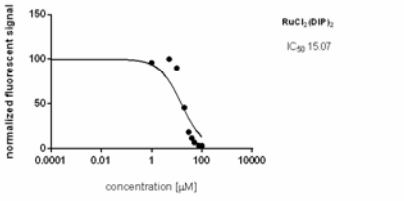

HeLa cytotoxicity replicate 2

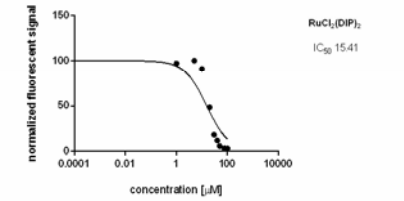

HeLa cytotoxicity replicate 3

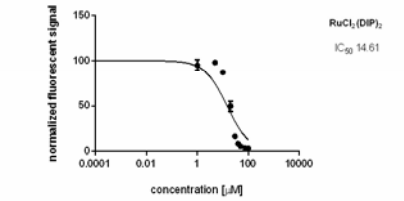

A2780 cytotoxicity replicate 1

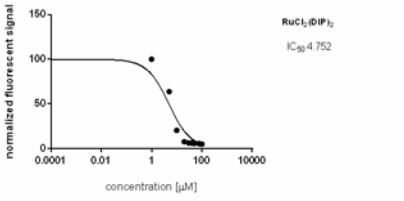

A2780 cytotoxicity replicate 2

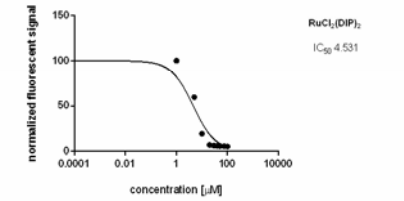

A2780 cytotoxicity replicate 3

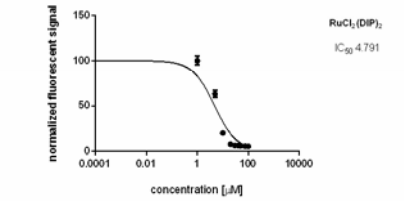

A2780 cis cytotoxicity replicate 1

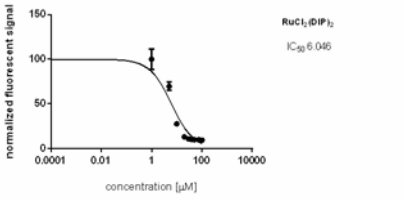

A2780 cis cytotoxicity replicate 2

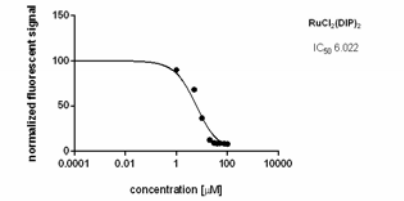

A2780 cis cytotoxicity replicate 3

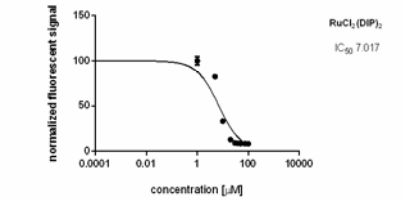

A2780 ADR cytotoxicity replicate 1

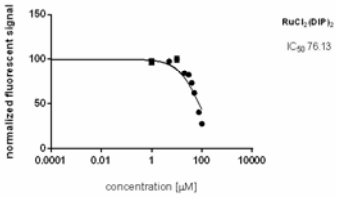

A2780 ADR cytotoxicity replicate 2

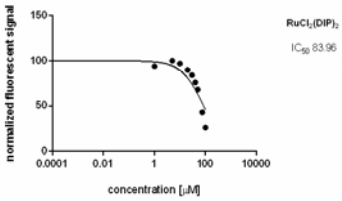

A2780 ADR cytotoxicity replicate 3

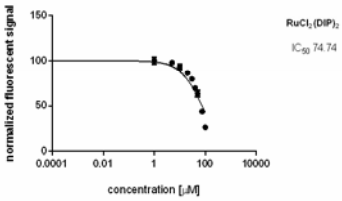

CT-26 cytotoxicity replicate 1

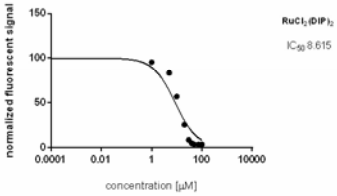

CT-26 cytotoxicity replicate 2

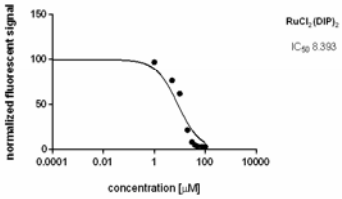

CT-26 cytotoxicity replicate 3

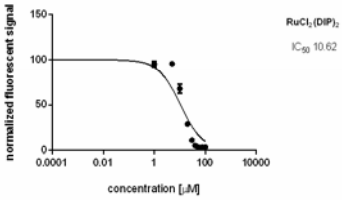

CT-26 LUC cytotoxicity replicate 1

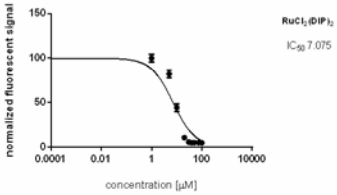

CT-26 LUC cytotoxicity replicate 2

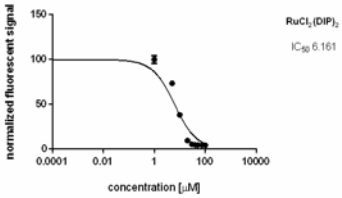

CT-26 LUC cytotoxicity replicate 3

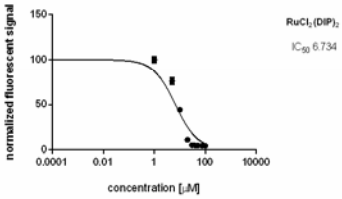

RPE-1 cytotoxicity replicate 1

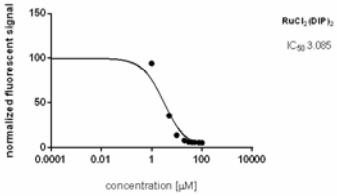

RPE-1 cytotoxicity replicate 2

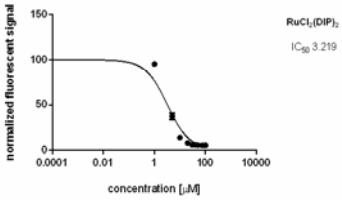

RPE-1 cytotoxicity replicate 3

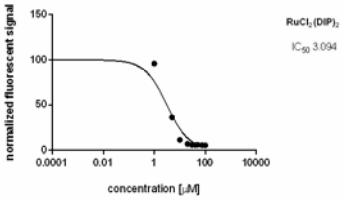

HeLa cytotoxicity replicate 1

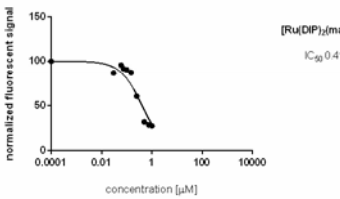

HeLa cytotoxicity replicate 2

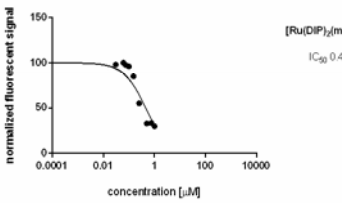

HeLa cytotoxicity replicate 3

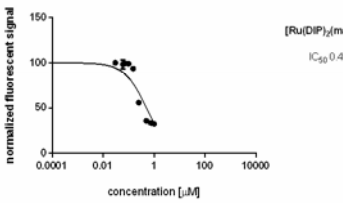

A2780 cytotoxicity replicate 1

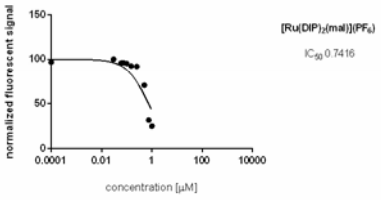

A2780 cytotoxicity replicate 2

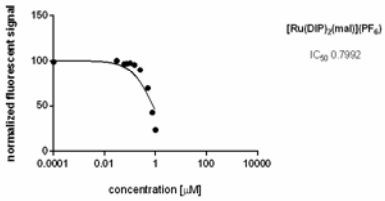

A2780 cytotoxicity replicate 3

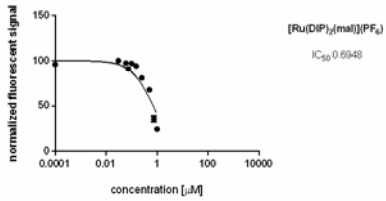

A2780 cis cytotoxicity replicate 1

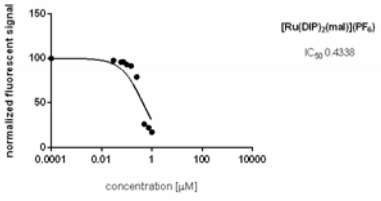

A2780 cis cytotoxicity replicate 2

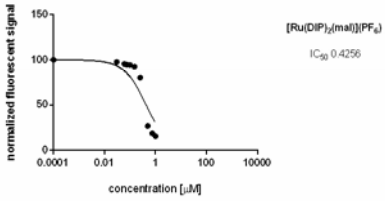

A2780 cis cytotoxicity replicate 3

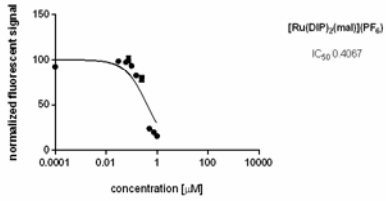

A2780 ADR cytotoxicity replicate 1

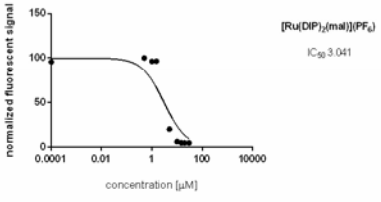

A2780 ADR cytotoxicity replicate 2

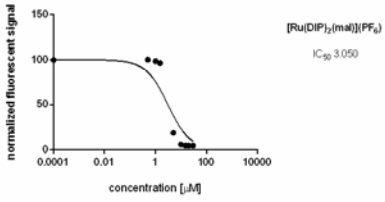

A2780 ADR cytotoxicity replicate 3

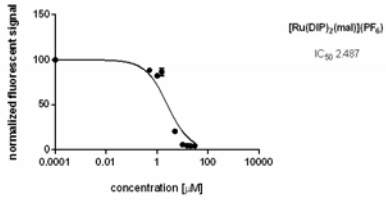

CT-26 cytotoxicity replicate 1

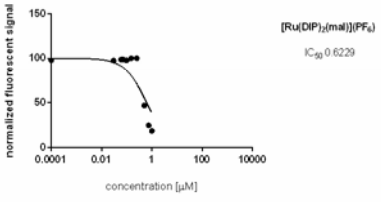

CT-26 cytotoxicity replicate 2

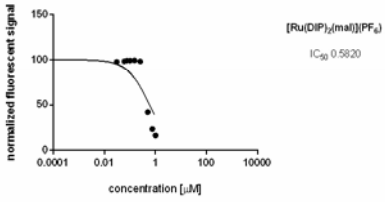

CT-26 cytotoxicity replicate 3

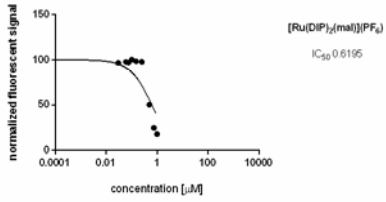

CT-26 LUC cytotoxicity replicate 1

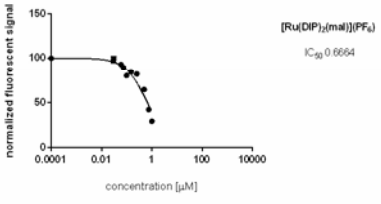

CT-26 LUC cytotoxicity replicate 2

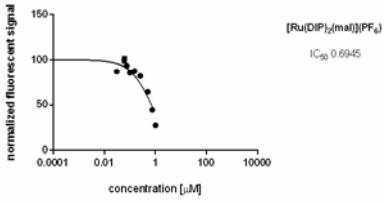

CT-26 LUC cytotoxicity replicate 3

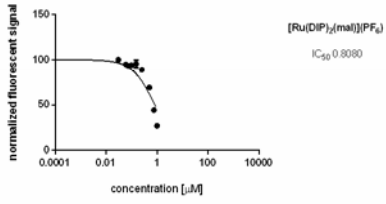

RPE-1 cytotoxicity replicate 1

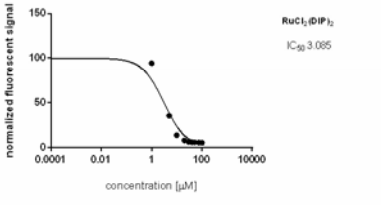

RPE-1 cytotoxicity replicate 2

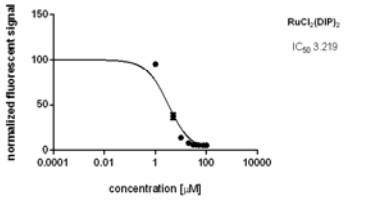

RPE-1 cytotoxicity replicate 3

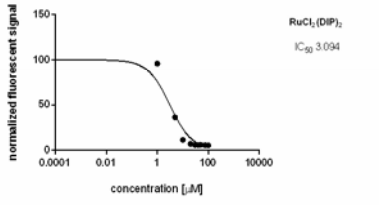

HeLa cytotoxicity replicate 1

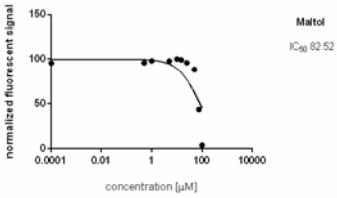

HeLa cytotoxicity replicate 2

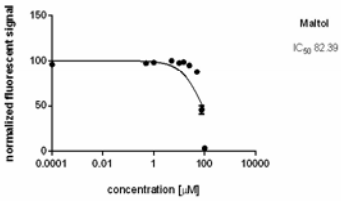

HeLa cytotoxicity replicate 3

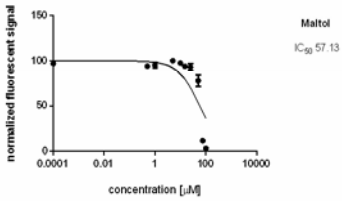

A2780 cytotoxicity replicate 1

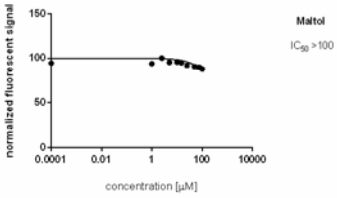

A2780 cytotoxicity replicate 2

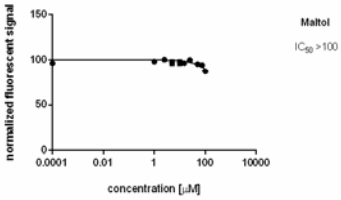

A2780 cytotoxicity replicate 3

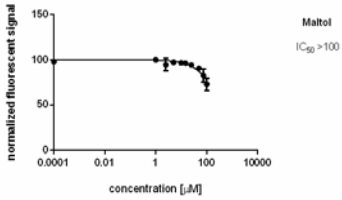

A2780 ADR cytotoxicity replicate 1

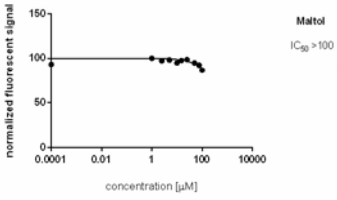

A2780 ADR cytotoxicity replicate 2

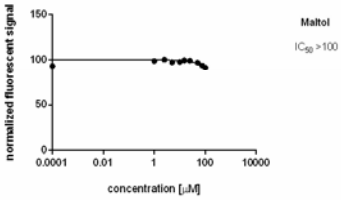

A2780 ADR cytotoxicity replicate 3

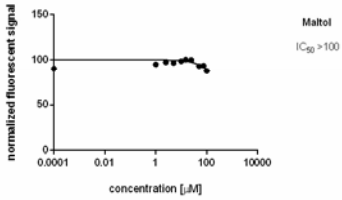

A2780 cis cytotoxicity replicate 1

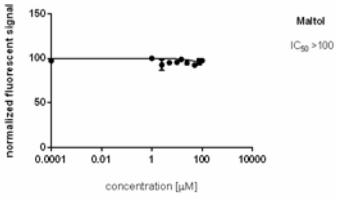

A2780 cis cytotoxicity replicate 2

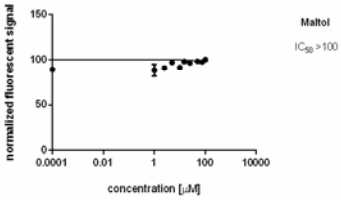

A2780 cis cytotoxicity replicate 3

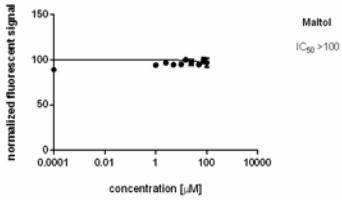

CT-26 cytotoxicity replicate 1

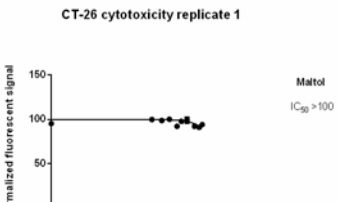

CT-26 cytotoxicity replicate 2

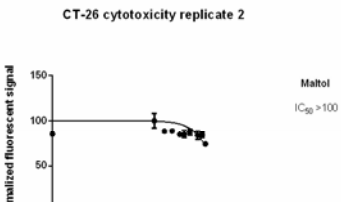

CT-26 cytotoxicity replicate 3

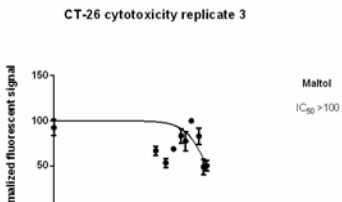

CT-26 LUC cytotoxicity replicate 1

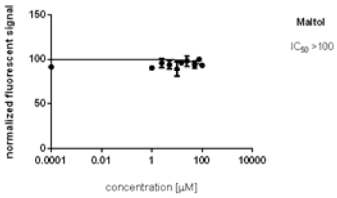

CT-26 LUC cytotoxicity replicate 2

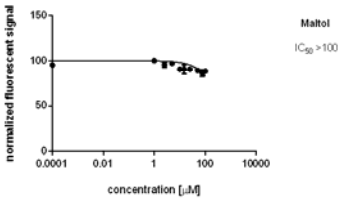

CT-26 LUC cytotoxicity replicate 3

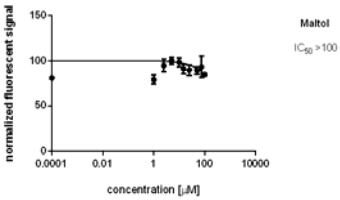

RPE-1 cytotoxicity replicate 1

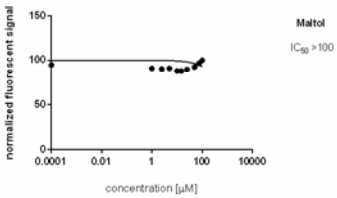

RPE-1 cytotoxicity replicate 2

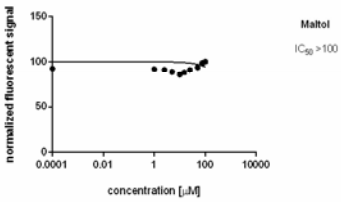

RPE-1 cytotoxicity replicate 3

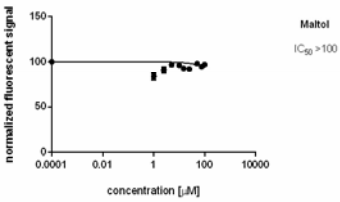

9) Figure S11. Evaluation of the cytotoxicity in 2D cell culture models *via* CellTiter Glo® viability Test.

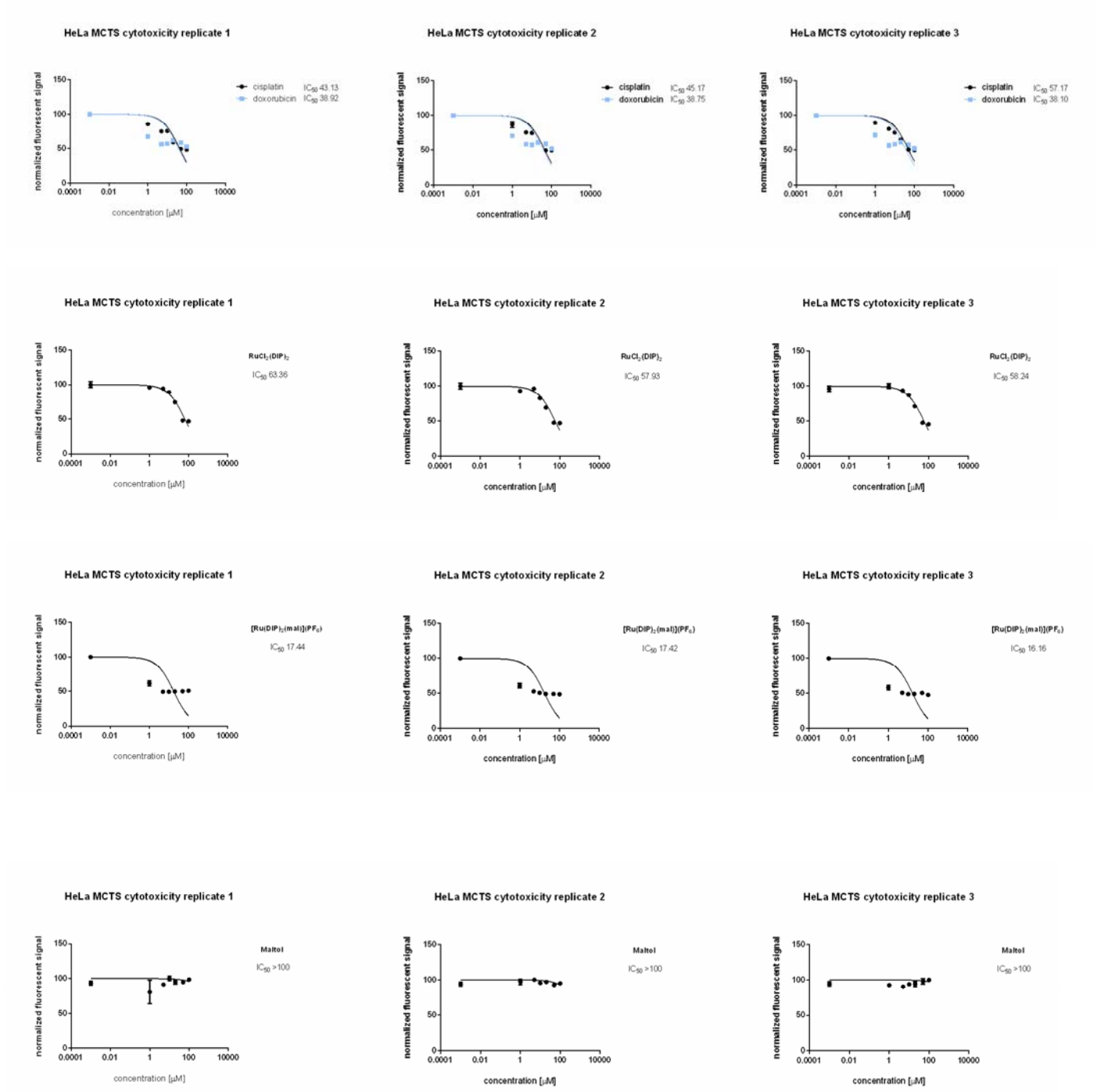

10) Figure S12. Cell Death Mechanism.

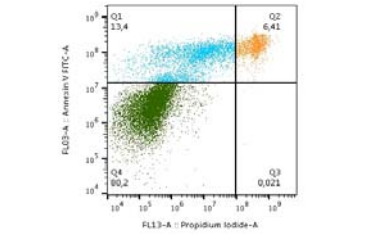

Sample Name	Subset Name	Count	Freq. of Parent
A6 Staurosporin 30 min.fcs	Q4: Propidium Iodide-A- , Annexin V FITC-A-	19114	80,2
A6 Staurosporin 30 min.fcs	Q3: Propidium Iodide-A+ , Annexin V FITC-A+	5,00	0,021
A6 Staurosporin 30 min.fcs	Q2: Propidium Iodide-A+ , Annexin V FITC-A+	1520	6,41
A6 Staurosporin 30 min.fcs	Q1: Propidium Iodide-A- , Annexin V FITC-A+	3190	13,4
A6 Staurosporin 30 min.fcs	Single Cells\fcs	23837	100,0

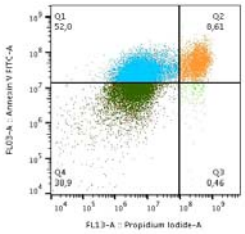

Sample Name	Subset Name	Count	Freq. of Parent
A7 staurosporin 4h.fcs	Q4: Propidium Iodide-A- , Annexin V FITC-A-	16245	38,9
A7 staurosporin 4h.fcs	Q3: Propidium Iodide-A+ , Annexin V FITC-A+	192	0,46
A7 staurosporin 4h.fcs	Q2: Propidium Iodide-A+ , Annexin V FITC-A+	3599	8,61
A7 staurosporin 4h.fcs	Q1: Propidium Iodide-A- , Annexin V FITC-A+	21752	52,0
A7 staurosporin 4h.fcs	Single Cells\fcs	41888	100,0

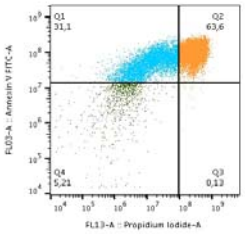

Sample Name	Subset Name	Count	Freq. of Parent
A8 staurosporin 24h.fcs	Q4: Propidium Iodide-A- , Annexin V FITC-A-	1003	5,21
A8 staurosporin 24h.fcs	Q3: Propidium Iodide-A+ , Annexin V FITC-A+	25,0	0,13
A8 staurosporin 24h.fcs	Q2: Propidium Iodide-A+ , Annexin V FITC-A+	12235	63,6
A8 staurosporin 24h.fcs	Q1: Propidium Iodide-A- , Annexin V FITC-A+	5979	31,1
A8 staurosporin 24h.fcs	Single Cells\fcs	19241	100,0

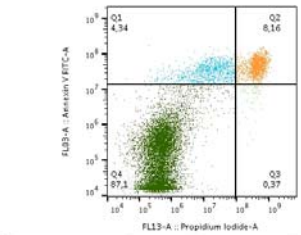

Sample Name	Subset Name	Count	Freq. of Parent
D4 (Rol(DIP)2ma(((IPF6) 30min.fcs	Q4: Propidium Iodide-A- , Annexin V FITC-A-	19171	87,1
D4 (Rol(DIP)2ma(((IPF6) 30min.fcs	Q3: Propidium Iodide-A+ , Annexin V FITC-A+	82,0	0,37
D4 (Rol(DIP)2ma(((IPF6) 30min.fcs	Q2: Propidium Iodide-A+ , Annexin V FITC-A+	1796	8,16
D4 (Rol(DIP)2ma(((IPF6) 30min.fcs	Q1: Propidium Iodide-A- , Annexin V FITC-A+	956	4,34
D4 (Rol(DIP)2ma(((IPF6) 30min.fcs	Single Cells\fcs	22005	99,9

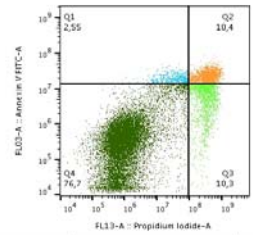

Sample Name	Subset Name	Count	Freq. of Parent
B5 (Rol(DIP)2ma(((IPF6) 4h.fcs	Q4: Propidium Iodide-A- , Annexin V FITC-A-	13193	76,7
B5 (Rol(DIP)2ma(((IPF6) 4h.fcs	Q3: Propidium Iodide-A+ , Annexin V FITC-A+	2042	10,3
B5 (Rol(DIP)2ma(((IPF6) 4h.fcs	Q2: Propidium Iodide-A+ , Annexin V FITC-A+	2069	10,4
B5 (Rol(DIP)2ma(((IPF6) 4h.fcs	Q1: Propidium Iodide-A- , Annexin V FITC-A+	505	2,55
B5 (Rol(DIP)2ma(((IPF6) 4h.fcs	Single Cells\fcs	19798	100,0

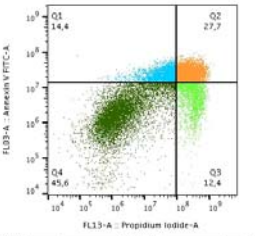

Sample Name	Subset Name	Count	Freq. of Parent
B6 (Rol(DIP)2ma(((IPF6) 24h.fcs	Q4: Propidium Iodide-A- , Annexin V FITC-A-	9394	45,6
B6 (Rol(DIP)2ma(((IPF6) 24h.fcs	Q3: Propidium Iodide-A+ , Annexin V FITC-A+	2551	12,4
B6 (Rol(DIP)2ma(((IPF6) 24h.fcs	Q2: Propidium Iodide-A+ , Annexin V FITC-A+	5698	27,7
B6 (Rol(DIP)2ma(((IPF6) 24h.fcs	Q1: Propidium Iodide-A- , Annexin V FITC-A+	2960	14,4
B6 (Rol(DIP)2ma(((IPF6) 24h.fcs	Single Cells\fcs	20603	99,9

11) Figure S13. Cellular uptake mechanism of **[Ru(DIP)$_2$(mal)](PF$_6$)**. Accumulation of ruthenium in HeLa cells in presence of different inhibitors and conditions: low temperature (4ºC), blocked cellular metabolism (2-Deoxy-*D*-glucose, oligomycin), blocked endocytic pathways (chloroquine or ammonium chloride), blocked cation transporters (tetraethylammonium chloride). Cells were pre-treated with uptake inhibitors and then incubated with **[Ru(DIP)$_2$(mal)](PF$_6$)** (2 h, 5 μM). Amounts of ruthenium were measured using ICP-MS.

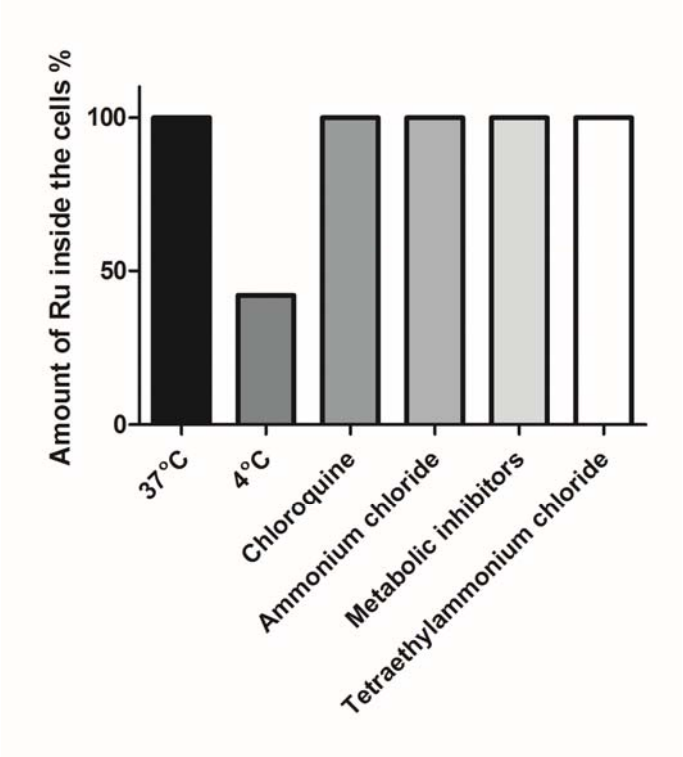

12) Figure S14. Oxygen consumption rates and different respiration parameters in HeLa cells alone or after treatment with various test compounds.

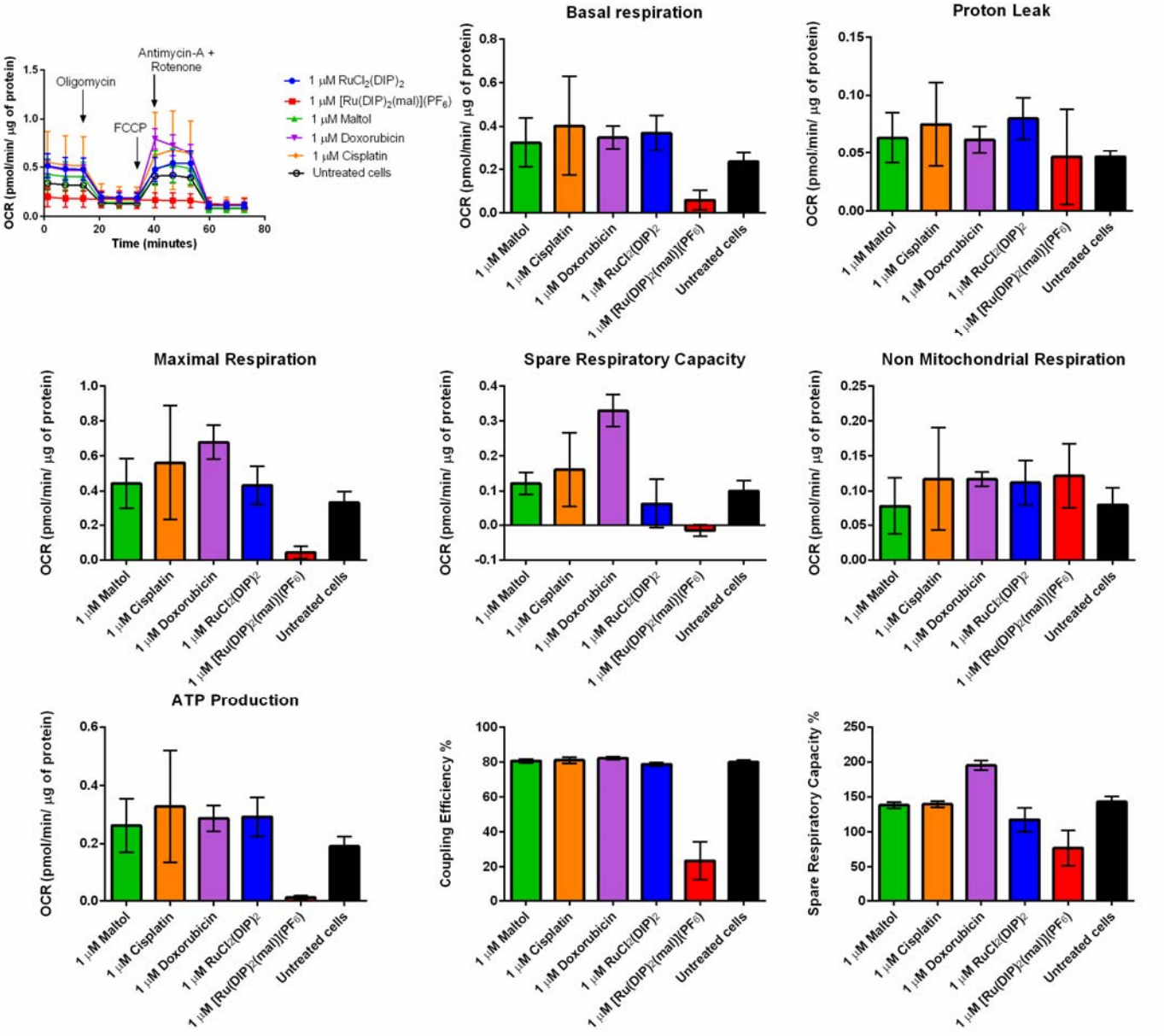

13) Figure S15. Extracellular acidification rate and different parameters during glycolysis in HeLa cells alone or after treatment with various test compounds.

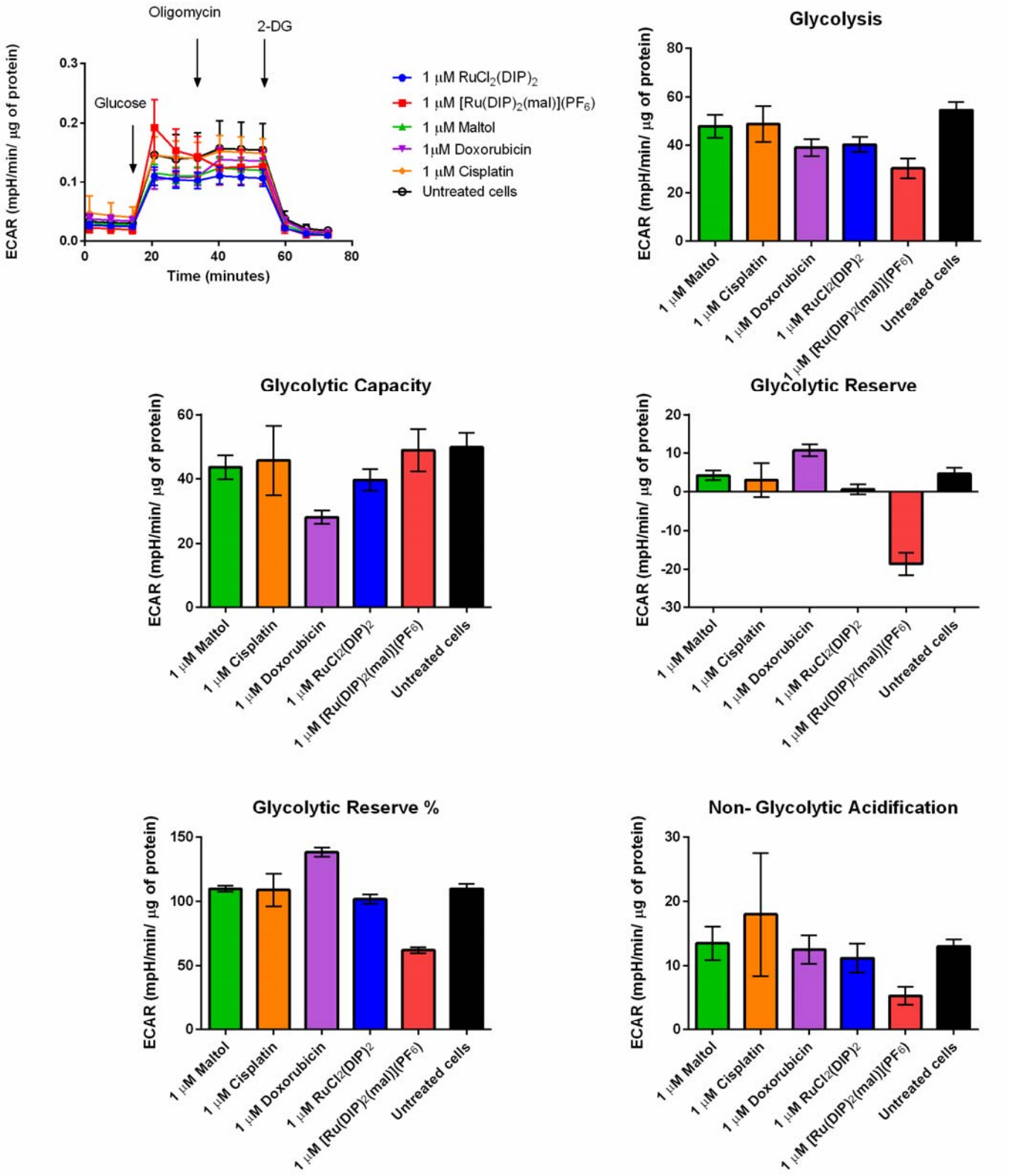

14) Figure S16. Fuel flex assay in HeLa cells. Dependency studies were performed by adding the inhibitor for the target pathway in port A and inhibitors for the other two pathways in port B while capacity studies were done using the reverse sequence. UK-5099 (20 μM), BPTES (30 μM) and etomoxir (40 μM) were used as the inhibitors for the fuel pathways run by glucose, glutamine and fatty acids.